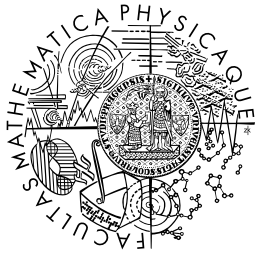

FACULTY
OF MATHEMATICS
AND PHYSICS
Charles University

MASTER THESIS

Hana Bušková

The presence and stability of DNA mini-hairpins

Department of Low-Temperature Physics

Supervisor of the master thesis: Mgr. Václav Římal, Ph.D.
Study programme: Biophysics and Chemical Physics
Study branch: Biophysics

Prague 2021

I declare that I carried out this master thesis independently, and only with the cited sources, literature and other professional sources. It has not been used to obtain another or the same degree.

I understand that my work relates to the rights and obligations under the Act No. 121/2000 Sb., the Copyright Act, as amended, in particular the fact that the Charles University has the right to conclude a license agreement on the use of this work as a school work pursuant to Section 60 subsection 1 of the Copyright Act.

In Prague, 22nd of July, 2021 .....

Author's signature

I would like to express my gratitude to my supervisor, Mgr. Václav Římal, PhD., for his enormous patience, and to my consultant doc. RNDr. Jan Lang, Ph.D. for providing valuable feedback. I would also like to thank my family, for giving me a helping hand, head, and ear, even when I didn't know I needed it.

Title: The presence and stability of DNA mini-hairpins

Author: Hana Bušková

Department: Department of Low-Temperature Physics

Supervisor: Mgr. Václav Římal, Ph.D., Department of Low-Temperature Physics

Abstract: The secondary structure of DNA is variable and depends on the sequence of nucleotides in a strand. While DNA can form duplexes, formations of three, four, or even a single strand have been observed *in vivo* and *in vitro* as well. In this thesis, we study the effect of small changes of oligonucleotide sequences on the stability of hairpins formed by DNA heptamers by ^{1}H nuclear magnetic resonance (NMR) spectroscopy. Suitable DNA sequences were selected based on symmetry rules and stability prediction by nearest neighbor model. Two-dimensional ^{1}H -^{1}H NOESY spectra were used to assign the ^{1}H resonances of aromatic hydrogens. Variable-temperature 1D spectra served for obtaining melting curves, from which the thermodynamic properties of the hairpins were determined. The presence of hairpins in the solutions was confirmed by the character of the NOESY spectra, independence of melting temperature on oligonucleotide concentration, and comparison of competing melting-curve models of duplex and hairpin. Our results point out the importance of the order of the stem base pairs and contribute to the description of the extraordinary stability of DNA mini-hairpins.

Keywords: NMR spectroscopy, DNA, hairpins

Contents

Introduction

Nucleic acids in nature achieve a high variety of secondary structures with up to four strands. Our interest lies in the single-stranded hairpins. Some sequences create highly stable hairpins with a strong dependence on nucleic base sequences. Perhaps that is why hairpins are a fairly common pattern in viral RNA[1][2].

The procaryotic replication bubble starts by the spontaneous cruciform formation (or, in other words, the formation of two hairpins) in the procaryotic replication bubble[3]. Likewise, in transcription, the ends of coding sequences in procaryotes often form hairpins, which cause the newly-formed RNA strand to fall off the RNA polymerase.

In humans, hairpin-forming sequences have been found to drive mutation in triple-repeat error prone regions of the DNA[4]. The presence of hairpins in the GGGCTA variant of proximal regions of telomeres[5] seems to be behind some instability of G4 quadruplexes. While we have found plenty of proof for the formation of hairpins in human DNA, they all seem to have disruptive effect that harms the organism more often than not. While there have been attempts to describe the rules by which the stability of a secondary structure is determined, they provide an estimate, rather than an accurate prediction.

Nuclear magnetic resonance (NMR) experiments are a useful method in this endeavor. The principle of NMR is vastly different from other spectral methods used in biophysics, and temperature varied experiments allow a glimpse into the melting process and thermodynamics of secondary DNA structures. NMR has its use especially in the realm of short oligonucleotides, where it allows us to calculate separate thermodynamic parameters for each nucleotide with precision.

The main goal of this thesis is to predict which seven bases long oligonucleotide sequences form stable hairpins, and to assign chemical shifts in selected DNA strands. Temperature varied NMR experiments will then describe the thermodynamic stability of the chosen samples, and we will use those to determine whether or not do the candidate strands indeed form the predicted hairpins.

1. Deoxyribonucleic acid

The primary structure of deoxyribonucleic acid (DNA) consists of three components. The phosphate backbone holds the chain together, the deoxyribose molecule in each nucleotide is responsible partially for conformation and partially for connecting the backbone and the nitrous base, and the base itself is the carrier of genetic information. The four major DNA bases, adenine, guanine, thymine and cytosine, are pictured in Fig. 1.1.

The numbering convention dictates that deoxyribose is labeled with primes (C1', C2', etc.), the nitrous bases are numbered as depicted in Fig. 1.1, and the nucleotides in a chain are indexed from 5' end to the 3' end. The nitrogen atoms in position 1 in pyrimidines and 9 in purines form a glycosidic bond with deoxyribose C1'. Each of the bases has 3 exposed edges for hydrogen bonding: the Watson–Crick edge (named after its role in canonical base pairing), the Hoogsteen edge (playing its role in an alternative base pairing), and the sugar edge (which is often sterically blocked from any pairings by the deoxyribose). Fig. 1.1 shows not only the convention for atom numbering, but also the naming of the edges.

1.1 Conformations of nucleotides

The degrees of freedom in a nucleotide are highlighted by the arrows drawn in Fig. 1.2. The glycosidic torsion angle χ has its energetic minima in the *syn* and *anti* conformations, with the base either above, or away from the deoxyribose, respectively[6]. These two distinct conformations expose different edges for potential hydrogen bonding.

The most common sugar puckers of the deoxyribose are 3'-endo, 3'-endo 2'-exo, 2'-endo 3'-exo, and finally, 2'-endo, where the endo carbons appear to be above the plane of the deoxyribose, and the exo below. The last are rotations around the bonds of the backbone, denoted by Greek letters α to ζ. All five dihedral angles of these bonds can rotate and influence the overall shape of the molecule, although free rotation is sterically blocked by the molecule.

Ab initio calculations on deoxynucleotides[6] have shown that even without a solvent, a single pyrimidine monophosphate has the lowest energy in the 3'-endo with the base in *syn* conformation.The energy difference favouring *syn* over *anti* conformation is even more pronounced in purine monophosphates due to steric blocking by the phosphate.

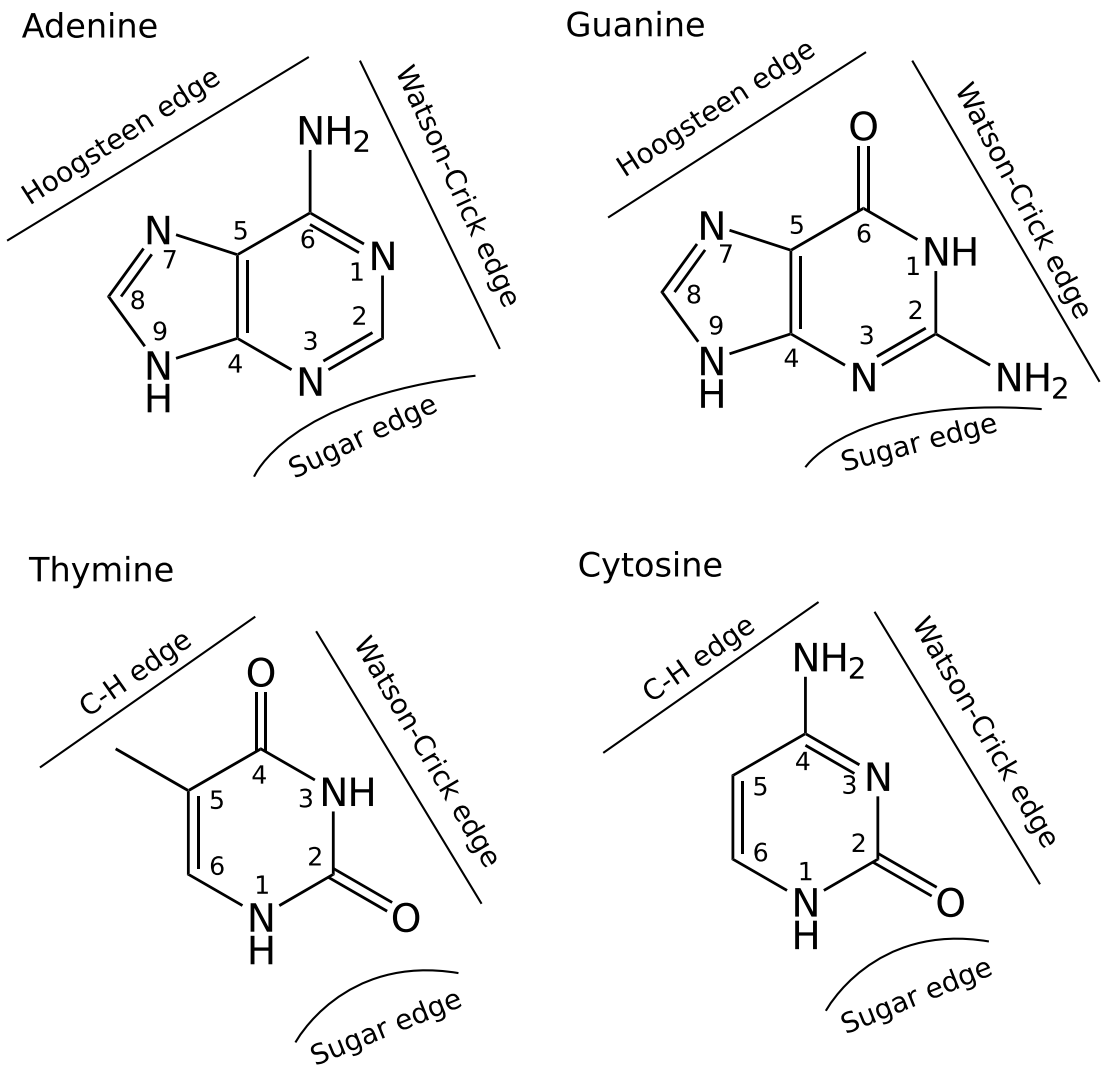

Figure 1.1: The four major bases of DNA. The C-H edge in pyrimidine bases is sometimes called Hoogsteen edge for the sake of consistency.

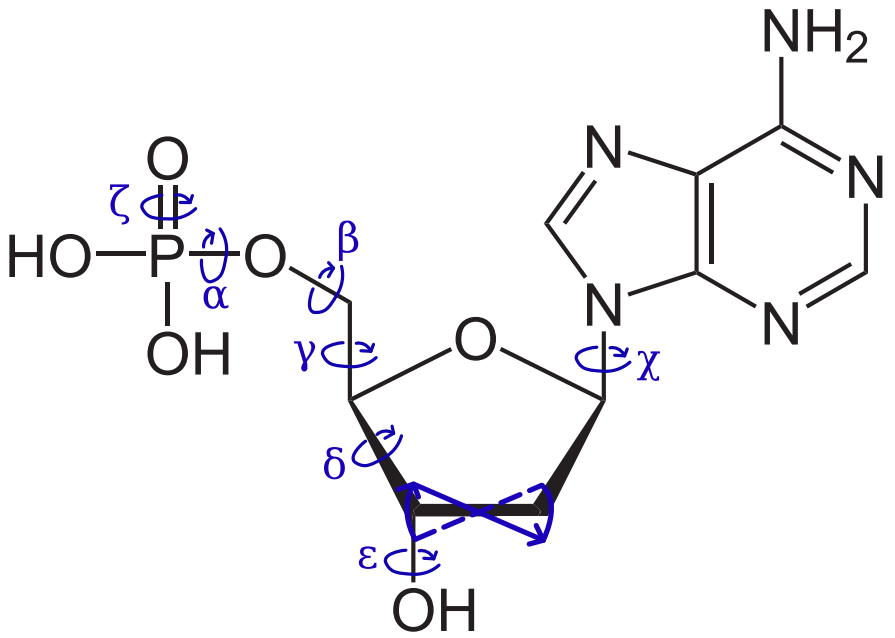

Figure 1.2: A schematic of a mononucleotide with degrees of freedom highlighted in blue.

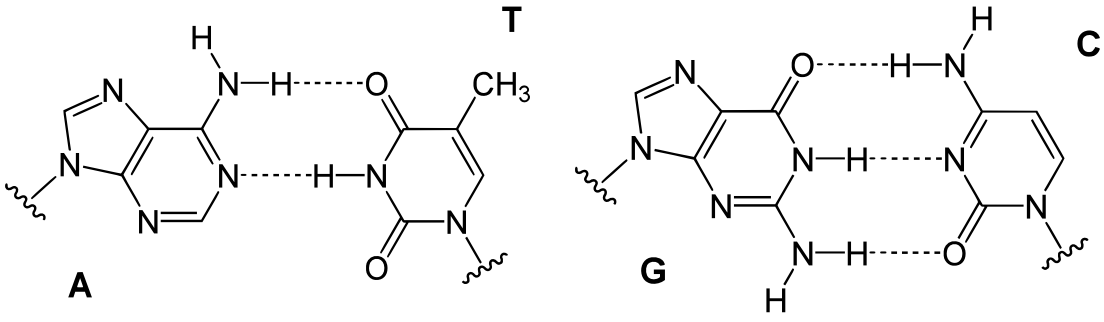

Figure 1.3: Watson–Crick canonical base pairing between complementary bases A·T and C·G

1.2 Secondary structure

The bases of two (or more) strands of DNA form hydrogen bonds, which hold the strands together. Those bonds usually form along the Watson-Crick edges (shown in Fig. 1.3), where cytosine pairs with guanine by three hydrogen bonds and adenine pairs with thymine by two bonds.

Pairs along other edges are common, and even more so in RNA. A nomenclature for the description of non-canonical base-pairing in RNA has been described by Leontis et al.[7][8], and lends itself well to DNA applications, too.

Another feature that stabilizes the overall secondary and tertiary structure of DNA is the stacking interaction among the aromatic rings of the bases. This even further ensures the stability of the resulting structure, as the most energetically favorable position for a base lies parallel and slightly off-axis to the aromatic ring of another one.

The secondary structure of the DNA molecule, or a complex of molecules, depends on the sequence of bases. Double helices, triple helices[9], guanine quadruplexes[10], hairpins, kissing complexes, and Holliday junctions[11], are just some of the tertiary structures that appear in nature, each with its own role in replication, recombination, or the regulation of gene expression.

1.3 DNA duplex

The most common *in vivo* secondary structure of DNA is B-DNA. Two molecules running in an anti-parallel direction form a double helix, connected by Watson-Crick pairing of the hydrophobic bases, protected from the outside environment by the phosphate backbone. The bases are in *anti* angle from the deoxyribose, which has the 3'-endo pucker. While B-DNA is the most common way the nucleic acid arranges itself in eucaryotic condensed chromatin, the crystalline A-DNA was the one first observed by Franklin[12]. Z-DNA, the only left-handed double helix, serves to relieve tension from untwisting DNA undergoing transcription further along the strand.

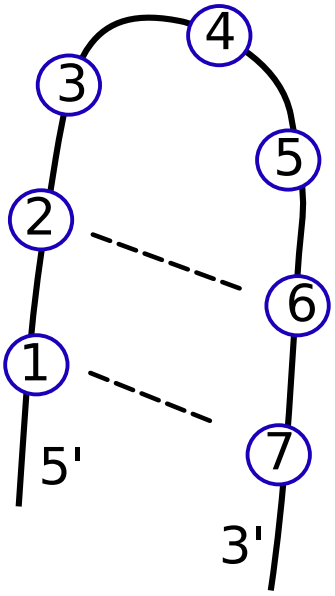

Figure 1.4: Simplified diagram of a 7-member minihairpin. The three bases 3, 4 and 5 form the loop, while the rest forms the base pairs N1·N7 and N2·N6.

1.4 Hairpin formation

Harpins (also stem-loops or hairpin loops) form by intramolecular hydrogen bonding between two regions of the same strand, forming a double-helical stem, and a loop. The hairpin may be of any length, but the shortest stable observed hairpins consist of a three bases long loop, and a stable stem from two base pairs. There is no upper limit to the length of the stem or the loop, provided the stem is stable enough to support the loop. Even 12 bases long sequences with 3 base pairs in the stem and 6 bases in the stem can form stable stem-loops[13][14]. An example hairpin is pictured in Fig. 1.4.

The spontaneous formation of hairpins at the end of the mRNA strand is the underlying mechanism for termination of transcription in procaryotes. In eucaryotic DNA, they play a role in triplet expansion mutations[15][16] by increasing slippage during replication.

Specific seven bases long oligomers have even been reported on. For example, the CGGTACG oligomer is the most common sequence on the 21st and 22nd chromosome in humans[17], and has been compared in molecular dynamics experiments with its close relative, GCGTAGC[18]. GCGTACG[19][20] and GCGAACG[21]have both been reported to form a duplex. Other sequences aid transcription in some way, one being AGGAACT at the start of a promoter for a transcription factor[22], and another, AGGCACG, engaging as part of the TATA box[23].

2. Thermodynamics of processes in an aqueous solution

2.1 General reaction in an aqueous solution

The general form of a reversible reaction in a dilute aqueous solution is

$$a\mathrm{A} + b\mathrm{B} \underset{k_{-1}}{\overset{k_1}{\rightleftharpoons}} c\mathrm{C} + d\mathrm{D} \tag{2.1}$$

where capital letters denote the reactants A, B, and the products C, D, and the miniscule letters denote their respective stoichiometric coefficients. The equilibrium constant for such a reaction is then given as

$$K = \frac{[\mathrm{C}]^c[\mathrm{D}]^d}{[\mathrm{A}]^a[\mathrm{B}]^b} \tag{2.2}$$

the dimension of which depends on the stoichiometric coefficients, and takes the general form of concentration to the power of a rational number. The temperature dependence of K is connected to the Gibbs free energy ΔG by the equation

$$\Delta G = \Delta H - T\Delta S \tag{2.3}$$

where ΔH and ΔS denote the change of enthalpy and entropy, respectively, and T is absolute temperature.

2.2 Two-state system with hairpin and single strand

A reaction between a denatured strand S and a hairpin H takes the form of

$$\mathrm{S} \rightleftharpoons \mathrm{H} \tag{2.4}$$

where the equilibrium constant follows to be

$$K = \frac{c_\mathrm{H}}{c_\mathrm{S}} \tag{2.5}$$

Concentrations can be converted to dimensionless populations, which have their sum normalized to one. Populations, rather than concentrations, are more appropriate for the description of chemical exchange in NMR. The total concentration and population of the oligonucleotide in the solution is the sum of the concentrations (or populations) on both sides,

$$c_0 = c_\mathrm{S} + c_\mathrm{H} \tag{2.6}$$

$$1 = p_0 = p_\mathrm{S} + p_\mathrm{H} \tag{2.7}$$

The population of the hairpin will then depend on the equilibrium constant, which itself is dependent on temperature:

$$p_{\mathrm{H}} = \frac{K}{1+K} \tag{2.8}$$

To obtain the melting temperature, we will require the van't Hoff equation

$$\Delta G = -RT \ln K \tag{2.9}$$

The melting temperature of a reversible system is defined as a temperature where half the molecules is in the product state and half in the reactant state, meaning that $K = 1$, and the Gibbs free energy $\Delta G = 0$. The melting temperature T_m of hairpins does not depend on concentration, but only on the enthalpy ΔH and the enthropy ΔS of the reaction:

$$T_m = \frac{\Delta H}{\Delta S} \tag{2.10}$$

2.3 Two-state system with duplex and single strand

For the formation of a duplex D from identical strands S,

$$2\mathrm{S} \rightleftharpoons \mathrm{D} \tag{2.11}$$

the equilibrium constant derived from Eq. 2.1 follows to be

$$K = \frac{c_{\mathrm{D}}}{c_{\mathrm{S}}^2} \tag{2.12}$$

Here, the population approach is more useful than the concentration approach. While the total concentration of oligonucleotide c_0 stays the same, the sum of concentrations c_S and c_D no longer equals c_0 for any $c_D > 0$. However, populations always sum up to one. The population approach highlights the fraction of total molecules, rather than the concentration. The relationships between concentrations and populations are:

$$p_{\mathrm{S}} = \frac{c_S}{c_0} \tag{2.13}$$

$$p_{\mathrm{D}} = 2\frac{c_D}{c_0} \tag{2.14}$$

The van't Hoff equation is slightly different from 2.9:

$$\Delta G = -RT \ln(c_{\mathrm{ref}} K) \tag{2.15}$$

The reference concentration c_{ref} may be arbitrarily chosen. In this thesis, we choose 1 M. R represents the universal gas constant. The van't Hoff equation linear in ΔH, ΔS is derived from the equations 2.3 and 2.15 as

$$\ln K = \frac{1}{c_{\mathrm{ref}}}\Big(-\frac{\Delta H}{RT} + \frac{\Delta S}{R}\Big) \tag{2.16}$$

The population of duplexes p_{D} can be calculated from the equations 2.16, 2.12, 2.13,2.14 and 2.15 as

$$p_{\mathrm{D}} = \frac{1 + \kappa - \sqrt{1 + 2\kappa}}{2\kappa}, \tag{2.17}$$

$$\kappa = \frac{4c_0}{c_{\mathrm{ref}}} \exp\left(\frac{-\Delta G}{RT}\right) \tag{2.18}$$

And finally, the melting temperature can be calculated as

$$T_m = \frac{\Delta H}{\Delta S - R \ln \frac{c_0}{c_{\mathrm{ref}}}} \tag{2.19}$$

2.4 Three-state system with duplex, hairpin, and single strand

A system which can form both hairpins and duplexes would have the following set of chemical equations,

$$2\mathrm{S} \rightleftharpoons \mathrm{D} \quad \text{and} \quad \mathrm{S} \rightleftharpoons \mathrm{H} \tag{2.20}$$

The populations still sum up to one, with their relationship to the concentrations as follows:

$$p_D = 2\frac{c_D}{c_0} \qquad p_S = \frac{c_S}{c_0} \qquad p_H = \frac{c_H}{c_0} \tag{2.21}$$

$$c_0 = 2c_D + c_S + c_H \tag{2.22}$$

$$1 = p_D + p_S + p_H \tag{2.23}$$

$$1 = 2\frac{c_D}{c_0} + \frac{c_S}{c_0} + \frac{c_H}{c_0} \tag{2.24}$$

The equilibrium constants for this set of equations are then

$$K_1 = \frac{c_D}{c_S^2} \tag{2.25}$$

$$K_2 = \frac{c_H}{c_S} \tag{2.26}$$

Together, the equations 2.23, 2.25 and 2.26 with the use of substitutions 2.21 give us the following populations, dependent only on the equilibrium constants (which themselves depend on the temperature)[24].

$$p_S = \frac{\sqrt{(K_2 + 1)^2 + 8c_0 K_1 c_{\mathrm{ref}}} - K_2 - 1}{4K_1 c_0 c_{\mathrm{ref}}} \tag{2.27}$$

$$p_D = 2K_1 c_0 p_S^2 \tag{2.28}$$

$$p_H = p_S K_2 \tag{2.29}$$

Not only do the thermodynamic parameters give us the required energies that can be used for further analysis of the processes of replication, transcription and DNA repair, but the melting temperature calculated can be used to distinguish among multiple possible secondary structures: the fit of the melting curve and the change of the melting temperature (or lack of thereof) with c_0 are a definitive proof of the formation of hairpins in the sample.

2.5 Nearest-neighbor model

Prediction of the aforementioned thermodynamic parameters has been attempted by multiple approaches. The most comprehensive one is the nearest neighbor model[25] which lies at the core of the DINAMelt[26] web server tool, which serves to predict the secondary structure of nucleic acids and their properties. The values for 10 possible variations of nearest neighbors are tabulated. The Gibbs free energy estimate is calculated as a sum of all nearest neighbor terms forming a pair, plus penalty for the ending base pair, among other terms. The nearest neighbor model serves as a good estimate of oligonucleotide secondary structure stability.

3. Nuclear Magnetic Resonance

Each atomic nucleus has a spin $\boldsymbol{I}$ and posesses a magnetic moment, $\boldsymbol{\mu}$, which relate to each other through the gyromagnetic ratio γ as

$$\boldsymbol{\mu} = \gamma \boldsymbol{I}. \tag{3.1}$$

The gyromagnetic ratio is a characteristic value tabulated for every isotope in its ground state. Examples of some nuclei used in biochemical applications of magnetic resonance are shown in Table 3.1. Note that the ^{12}C isotope has been omitted due to its spin 0.

The spin $\boldsymbol{I}$ has properties of a quantum angular momentum. Each particle with a spin has $2I + 1$ degenerate energy levels. This degeneration is removed by the presence of a magnetic field, $\boldsymbol{B_0}$ by Zeeman effect. Let us assume a homogenous $\boldsymbol{B_0} = (0, 0, B_0)$. The difference between two adjacent energy levels in this magnetic field can be expressed as

$$\Delta E = \gamma B_0 \hbar. \tag{3.2}$$

At equilibrium, nuclei within the field B_0 are distributed on energy levels according to the Boltzmann distribution. The sum of magnetic moments of N nuclei in a given sample, nuclear magnetization $\boldsymbol{M}_0$, follows from Curie's law and the Boltzmann distribution as

$$\boldsymbol{M_0} = \frac{NI(I+1)\hbar^2\gamma^2}{3kT}\boldsymbol{B_0}. \tag{3.3}$$

3.1 Bloch equations

The macroscopic nuclear magnetization $\boldsymbol{M}$ interacts with the magnetic field according to the Bloch equations:

$$\frac{\mathrm{d}M_x}{\mathrm{d}t} = \gamma(\boldsymbol{M} \times \boldsymbol{B})_x - \frac{M_x}{T_2} \tag{3.4}$$

$$\frac{\mathrm{d}M_y}{\mathrm{d}t} = \gamma(\boldsymbol{M} \times \boldsymbol{B})_y - \frac{M_y}{T_2} \tag{3.5}$$

$$\frac{\mathrm{d}M_z}{\mathrm{d}t} = \gamma(\boldsymbol{M} \times \boldsymbol{B})_z - \frac{M_z - M_0}{T_1} \tag{3.6}$$

where T_1 denotes the longitudinal relaxation time, T_2 the transversal relaxation time, and M_0 is the equilibrium nuclear magnetization.

Table 3.1: Example isotopes and their respective gyromagnetic ratios[27]

Isotope	Spin I	γ [10^6rads^{-1}T^{-1}]	Natural abundance [%]
^{1}H	1/2	257.522	99.972
^{2}H	1	41.066	0.015
^{13}C	1/2	67.273	1.1
^{14}N	1	19.338	99.6
^{15}N	1/2	-27.126	0.37
^{31}P	1/2	108.394	100

3.2 Free induction decay

The simplest pulse-NMR experiment is a hard pulse along the x-axis, which turns the magnetization vector $\boldsymbol{M}$ by 90° from $(0, 0, M_0)$ to $(0, -M_0, 0)$. After the pulse, the magnetization vector precesses while relaxing back into M_0. As the system relaxes back into equilibrium, the longitudal magnetization $M_{\parallel}$ builds back up

$$M_{\parallel} = M_z = M_0(1 - e^{-\frac{t}{T_1}}) \tag{3.7}$$

and the transverse magnetic relaxation is detected by coil as FID with Larmor frequency ω_0:

$$M_{\perp} = M_0 e^{-i\omega_0 t + \phi} e^{-\frac{t}{T_2}} \tag{3.8}$$

The term $e^{i\omega_0 t}$ in $M_{\perp}(t)$ in Eq. 3.8 describes precession of the magnetization around the z axis. If only the static field $\boldsymbol{B_0} = (0, 0, B_0)$ is present, each of the nuclei individually undergoes free precession with Larmor frequency, also known as frequency of the free precession of magnetization. It follows from the Bloch equations and depends on the magnetic field $\boldsymbol{B_0}$ and the gyromagnetic ratio of the nucleus,

$$\omega_0 = -\gamma B_0 \tag{3.9}$$

The Fourier transform of Eq. 3.8 is the complex spectrum, $S(\omega)$, with its real and imaginary parts being the absorption and the dispersion Lorentz curves, respectively. The full width at half-maximum for an ideal spectral line is equal to $2/T_2$. Faster relaxation therefore leads to line broadening. The following equation describes the complex lorentzian[27]:

$$\mathcal{L}(\omega; \omega_0, T_2) = \frac{1}{1/T_2 + i(\omega - \omega_0)} \tag{3.10}$$

Its real part, the absorption lorentzian, follows:

$$\mathcal{A} = \frac{\lambda}{(1/T_2)^2 + (\omega - \omega_0)^2} \tag{3.11}$$

All of the above implies that the magnetic field $\boldsymbol{B_0}$ is perfectly homogenous, which of course cannot be the case. Spectral lines are subject to broadening due to field gradients. Their T_2^* is shorter than T_2 according to the following equation:

$$\frac{1}{T_2^*} = \frac{1}{T_2} + \gamma \Delta B_0 \tag{3.12}$$

where ΔB_0 denotes the difference in the magnetic field strength.

3.3 Chemical shift

The total magnetic field $\boldsymbol{B}$ influencing the Larmor frequency of the nucleus comprises from the external field $\boldsymbol{B}_0$ and the shielding by surrounding electrons, which

is generally a tensor, σ_{ij}. In liquid samples of low viscosity, only the isotropic shielding σ determines the spectral shape:

$$\sigma = \frac{1}{3}\mathbf{Tr}(\boldsymbol{\sigma}). \tag{3.13}$$

The angular resonance frequency of a nucleus with the shielding effect changes by $\gamma\sigma B_0$, to

$$\omega = \gamma(1-\sigma)B_0. \tag{3.14}$$

As the usual difference in ^{1}H spectra of diamagnetic compounds is in the range of 10^{-6} of the original frequency, chemical shift δ is expressed as units of ppm (parts per million), relative to the frequency of a standard ω_s:

$$\delta = \frac{\omega - \omega_\mathrm{s}}{\omega_\mathrm{s}} \tag{3.15}$$

3.4 Dipole-dipole interaction

The direct dipole-dipole interaction is due to the direct interaction between the magnetic moments of two nuclei. In isotropic liquids, the rotation of molecules during experiments time-averages the contribution of dipole-dipole interaction to zero.

Indirect dipole-dipole interaction, or J-interaction, is propagated by electron orbitals, introducing the requirement of chemical bonds. This causes a splitting of a single peak into a multiplet of $n+1$ peaks with binomial ratios in case of n equivalent J-couplings. The number of peaks in the multiplet is equal to the number of equivalent coupled nuclei plus one, with integrals of said peaks in binomial ratios to each other. Three-bond J-coupling for ^{1}H in organic molecules is approximately 7 Hz.

Both the chemical shift and the multiplicity of a signal from a nucleus can help in determining its position in a given molecule.

3.4.1 Nuclear Overhauser effect

The Nuclear Overhauser Effect (NOE) is related to the spin-lattice relaxation. Cross-relaxation between two nuclei is induced by their direct dipole-dipole interaction.

Among other uses, a NOESY experiment with optimal signal build-up can be used to distinguish between *trans* and *cis* isomers of simple organic molecules, or measurement of inter-proton distances.

NOE does have other applications (most notably, using ^{1}H cross-relaxation to enhance peaks in ^{13}C spectra[27]), but we are most interested in its ability to show cross-relaxation between two spatially close ^{1}H nuclei.

3.4.2 2D NOESY

The NOESY sequence, consisting of three 90° pulses, the evolution time t_1, and the mixing time t_m, is depicted on Fig. 3.1. A second dimension is introduced into NMR spectra through the change of a parameter in a set of 1D experiments.

^{1}H – ^{1}H NOESY (Nuclear Overhauser Effect SpectroscopY) varies the evolution time t_1. By applying Fourier transform on the t_2 dimension on the resulting free induction decays (FIDs) we obtain a set of 1D spectra. Transforming these further across the t_1 dimension results in a 2D spectrum. Off-diagonal crosspeaks at coordinates (δ_1, δ_2) can appear for nuclei with chemical shifts δ_1 and δ_2, if they are coupled by a direct spin-spin interaction. Therefore, spatial proximity of two atoms can be identified. Following up the NOESY sequence with water suppression techniques allows us to obtain 2D spectra with nearly negligible solvent signal.

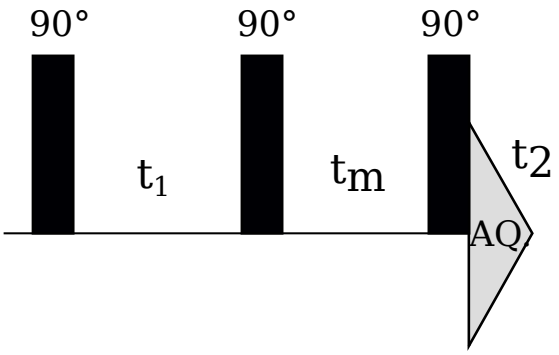

Figure 3.1: NOESY sequence diagram

3.5 Chemical exchange

NMR spectroscopy can be used to observe processes the sample may undergo. A chemical reaction, or even a conformational change may inadvertently cause a change in the chemical shift of a particular nucleus. These two different frequencies, Ω_A and Ω_B result in two distinct spectral lines if the rate constant k of the process is significantly smaller than their difference Ω_Δ, but these spectral lines draw closer to each other as the system approaches the intermediate exchange regime at $k \approx \Omega_\Delta$, and coalesce to a broad spectral line with high T_2^*. With increasing rate constant (typically from changes in temperature, concentration, or amount of available enzyme), the process enters the fast exchange regime, resulting in a narrow spectral line (Fig. 3.2). The new spectral line has the frequency of the weighted mean

$$\Omega = \Omega_\mathrm{A} p_\mathrm{A} + \Omega_\mathrm{B} p_\mathrm{B} \tag{3.16}$$

where p_A and p_B are the populations of the two species.

An $S \rightleftharpoons H$ system, as outlined in section 2.2, is an example of chemical exchange. Assuming that chemical shifts of nuclei in both hairpin and unfolded state follow linear dependence on temperature, the general form of the dependence of chemical shift on temperarure under fast chemical exchange can be expressed as

$$\delta = (aT + b)p_\mathrm{H} + (cT + d)(1 - p_\mathrm{H}). \tag{3.17}$$

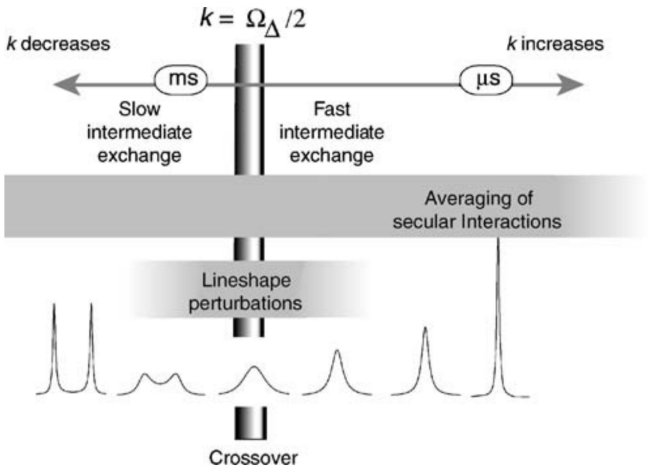

Figure 3.2: Two-site chemical exchange lineshape is dependent on the rate constant k relative to the angular frequency difference Ω_Δ. Reproduction from [27].

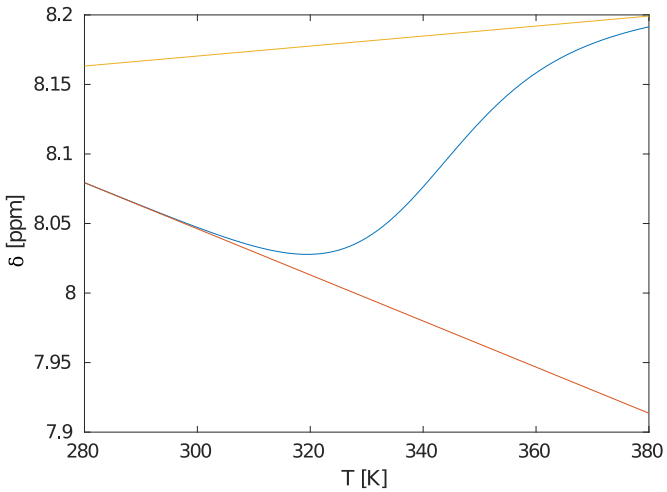

Figure 3.3: A demonstration of a generalized sigmoid curve calculated from Eq. 3.17, with asymptotes (red and yellow) that are not necessarily parallel. The asymptotes show the chemical shift of the two species if the system did not undergo chemical exchange.

Note that the $1 - p_H$ term here is equal to p_S, as the sum of populations is always equal to one. An example of such generalized sigmoid curve is provided in Fig. 3.3.

In a fast chemical exchange of the system in Eq. 2.20, the chemical shifts' behavior is analogous to the one outlined for hairpins in Eq. 3.17.

$$\delta = (a_D T + b_D)p_D + (a_S T + b_S)p_S + (a_H T + b_H)p_H \tag{3.18}$$

3.6 Spin echo

If after excitation and a $\tau/2$ delay, 180° inversion pulse is applied, the spins rephase back and a spin–echo signal is observed after a further $\tau/2$ delay. The echo signal has amplitude multiplied by $e^{-\tau/T_2}$ compared to a FID taken right after the excitation pulse. Spin echo has its use in the refocusing of chemical shift

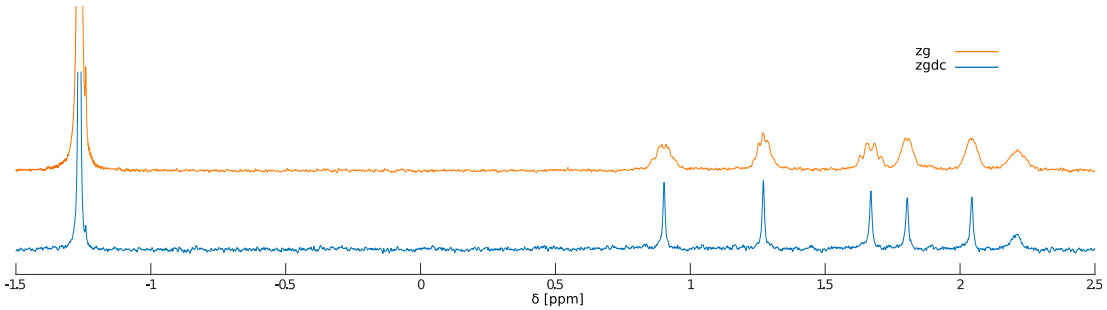

Figure 3.4: Comparison of decoupled and undecoupled NMR spectra of ^{31}P nuclei of 1.15 mM d(GCGTAGC) at 298 K.

in composite NMR sequences.

3.7 Decoupling

Suppressing the effect of J-coupling can be achieved by continuous irradiation, or more often composite pulse decoupling, of the coupled nuclei. The result is a spectrum similar to the non-decoupled spectrum, but with multiplets replaced by single peaks. Fig. 3.4 demonstrates a comparison between the spectra.

3.8 Solvent suppression

Suppressing the signal of solvent may be desirable in experiments with low solute concentrations.

3.8.1 Presaturation

In presaturation, the ^{1}H solvent Larmor frequency is continuously irradiated, equalizing the populations of its energy levels.

Presaturation also has the effect of completely eliminating the signal of exchangeable protons from the NMR spectrum.

3.8.2 Excitation sculpting with gradients

This method, first outlined in 1995[28] as part of the WATERGATE (WATER suppression by GrAdient Tailored Excitation) family[29], uses a pair of gradient pulses at the frequency of the solvent ^{1}H nuclei. The first gradient pulse dephases the spectrum. It is then followed by a set of pulses that are equivalent to 180° pulse for the rest of the sample, but not for the solvent. As a result, the second gradient pulse refocuses all the spins, except for the solvent.

The equivalent 180° pulse is usually done in two ways, represented by the zgesgp, and zggpw5 sequences on Fig. 3.5. The first is a Gauss pulse tuned to the suppressed frequency, followed by a hard 180° pulse. The second achieves the same goal with a binomial train of hard pulses, which again sum up to 180°. The other nuclei undergo the same process as they would do in a spin echo, but the water signal is dephased and suppressed.

While there are other techniques of solvent suppression, the shortest WATERGATE class sequences can achieve that task in a short timespan: that means the exchangeable protons (in -OH and -NH groups) have lower likelihood of being exchanged with the solvent in the time between excitation and measurement. Their signal may be visible with this technique, even if it is completely suppressed in others.

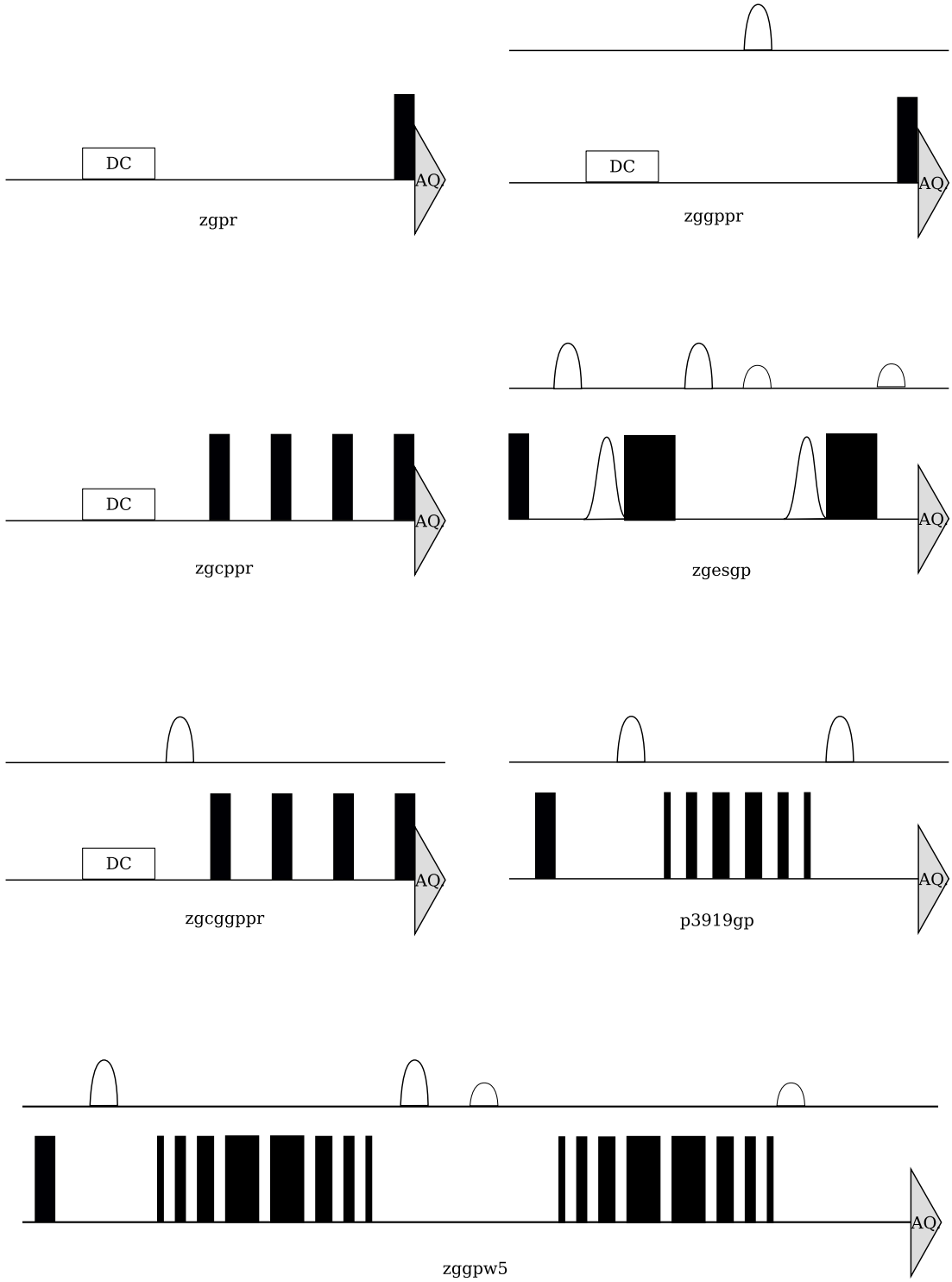

Figure 3.5: NMR sequences of interest from Bruker sequence catalog[30]

4. Materials and Methods

4.1 Sample preparation

We prepared two different solutions, which were mixed to achieve $pH = 7$: one solution contained Na_2HPO_4, while the second was prepared with NaH_2PO_4. Solutions included NaCl, so that the concentrations of Na^+ would be equal in both. The resulting buffer solution consisted of 25 mM PO_4^{3-} and 200 mM Na^+ in 10% D_2O and 90% H_2O. The NMR standard used was DSS with the IUPAC name 3-(trimethylsilyl)propane-1-sulfonate. Fully deuterated 0.8μM EDTA was added to ensure chelation of any unwanted polydentate metal ions.

The DNA oligonucleotides were purchased from the Faculty of Science of Masaryk University, Brno, Czech Republic, where they were prepared on an Expedite Nucleic Acid Synthesis System. They were HPLC purified and five times lyophilized by the producer. These samples were dissolved in the buffer solution specified above.

Two sequences of DNA which differ by the order of the first two base pairs, CGGTACG (referred to as Charlie) and GCGTAGC (henceforth referred to as George) were each dissolved in 0.6 ml of the buffer solution, resulting in approximately 1 mM solutions of each. The exact concentrations may be found in table 4.1.

4.2 NMR spectroscopy

All spectra were measured on the spectrometer Bruker Avance III HD, with magnetic field 11.7 T, which corresponds to the ^{1}H resonance frequency 500.13 MHz. The experiments were undertaken with the BBFO probe, a broadband probe capable of automatic shimming, as well as tuning and matching.

4.2.1 Water suppression optimization

The spectra were measured on a 2.5 mM sample of CTTm^{5}CGAAG, with $pH = 7$ buffer solution of 75 mM PO_4^{3-} and 200 mM Na^+ with 10% D_2O solvent and DSS as an internal standard. No EDTA was used in this case. Three pulse experiment families were investigated: presaturation (zgpr, zggppr, zgcpgppr), WATERGATE with a single pair of gradients (p3919gp), and WATERGATE with two pairs of gradients (zgesgp, zggpw5). All experiments were done with 4 scans preceded by 4 dummy scans. The presaturation relaxation delay (D1) was 3 seconds, and WATERGATE D1 was 1 second.

4.2.2 Determination of concentration by ^{31}P NMR

The concentration was determined from a zg experiment on the ^{31}P nuclei. 1000 scans (NS) and no dummy scans were taken, each with 2 seconds of acquisition tome over 16384 points of the time domain (TD). Relaxation delay (D1) was 60 seconds between measurements.

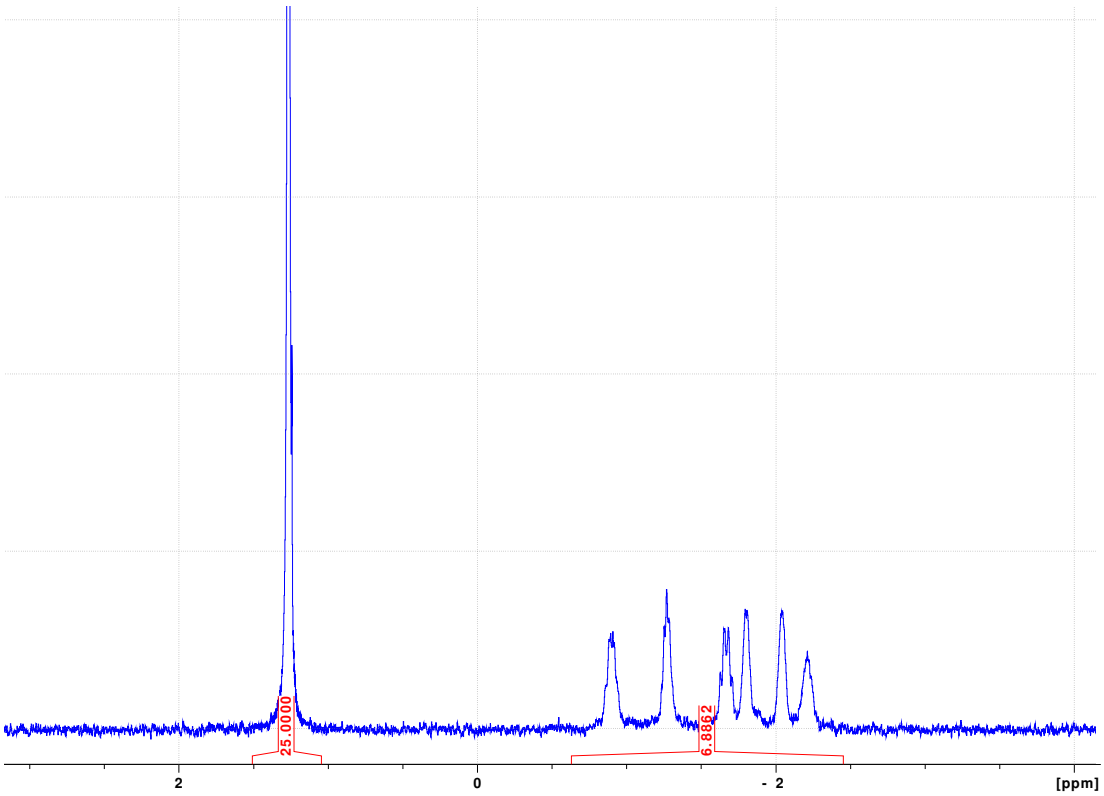

Figure 4.1: Concentration determination in the George sample from known concentration of inorganic phosphate. The oligonucleotide contains 6 phosphates in its backbone.

Table 4.1: Samples used

sample name	DNA sequence	concentration
Charlie	CGGTACG	1.66 mM
Charlie 0.2	CGGTACG	0.28 mM
George	GCGTAGC	1.15 mM

The concentration was then calculated from the ratios of the sum of the area under phosphate peaks in the DNA backbone, and the inorganic phosphate. A George ^{31}P spectrum is shown on Fig. 4.1. The concentrations of the samples are in the table 4.1

4.2.3 Peak assignment strategy of the aromatic region of spectra with NOESY

The sequence used for the NOESY spectra, composed of NOESY and water suppression by excitation sculpting with gradients, can be seen on Fig. 4.2. A typical ^{1}H NOESY spectrum is shown in Fig. 4.3. Two regions, highlighted here by red rectangles, are of interest. Both of these regions contain crosspeaks between sugar ^{1}H nuclei and aromatic ^{1}H nuclei. The area around 2 ppm is a region of H2' and H2" chemical shifts, while the space around 6 ppm contains mostly H1'. Each of the peaks in the 1D spectrum in the aromatic region (7-8.5 ppm) of B-DNA, except for the one belonging to the first residue, should

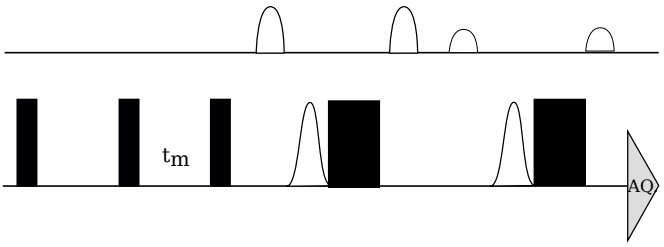

Figure 4.2: Pulse sequence used in peak assignment, noesyesgpph.

have 1 intraresidual H1' cross-peak and 1 interresidual H1' cross-peak. The same applies to H2' and H2" cross-peaks[31].

The task of assigning the aromatic signals becomes simpler in samples that have one very distinct nucleus. This is our case in both sequences, where thymine is represented exactly once. As thymine H6 has a chemical shift between 7.4 and 7.2 ppm, it is alternatively possible to trace in both directions from it, rather than having to search for the beginning or the ending aromatic atom. The assignment of the thymine is further supported by crosspeaks to its methyl group, and weak J-coupling to methyl hydrogens in well-resolved spectra. Moreover, cytosine H6 signals can be easily distinguished from other aromatic atoms, because they form doublets due to their J-coupling with H6 protons. Adenine H2 signals can be identified by their missing crosspeaks with deoxyribose in NOESY spectra. As we didn't use oligonucleotides with multiple adenines, it wasn't necessary to develop a method of discerning among different adenine H2 signals.

4.2.4 Temperature-dependent ^{1}H spectra

Variable temperature NMR experiments allow us to extract the information about the stability of the samples. 47 spectra were measured for each sample for the temperature range 274-366 K, with a step of 2 K. We have used the shortest possible pulse sequence, namely p3919gp, in order to achieve higher intensity of broad ^{1}H signals.

The spectra were obtained at 300 l/h flush gas flow through the probe, and 1200 l/h gas flow through the shim circuit in all temperatures of the sample to prevent variation. Between measurements at different temperatures, 15 minute waiting period was inserted to equalize temperature across the sample. Tuning, matching and shimming were done by automatic procedures right before the measurements were taken. NS 1024, TD 65536, and D1 1 second for George and Charlie samples. For the Charlie 02 sample, the NS was increased to 2048.

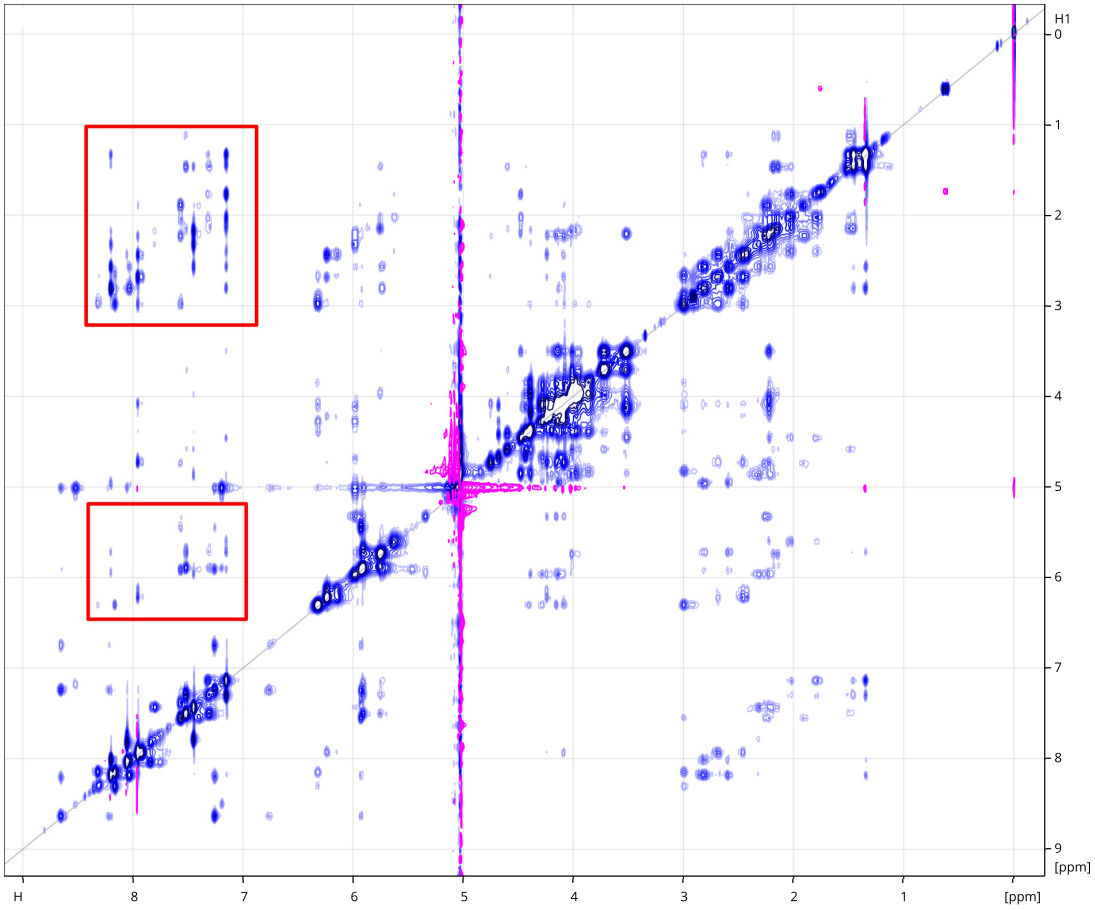

Figure 4.3: Charlie at 278 K, an example of a NOESY spectrum of DNA with suppressed aqueous solvent.

5. Results

5.1 Water suppression sequences

Six pulse sequences in total were examined. The p3919gp (with a full example spectrum shown on Fig. 5.1) was ultimately chosen due to being an optimal compromise between water suppression, amplitude distortion in the water region (Fig. 5.3), and suppression of exchangeable hydrogens (visible on Fig. 5.3 and 5.4). Furthermore, the short echo time allows superior resolution of hydrogens with broad signal, such as the one pictured on Fig. 5.2. The trade-off of poor phasing of the residual water peak in the p3919gp experiment was deemed acceptable, as we gained the signals of nuclei invisible to slower methods.

5.2 Selection of DNA sequences as hairpin candidates

Only oligonucleotides with seven bases, the smallest possible hairpin, were considered in this thesis. Out of those, the search had to be narrowed even further. The sequences were chosen according to the following criteria based on canonical base pairing, in order to minimize the probability of encountering other, undesirable secondary structures.

- The 1st and 2nd base must be complementary to the 7th and 6th, respectively. That narrows the search to five unique base combinations, resulting in 4^5=1024 possibilities.
- Out of the 1024, 32 candidates (for example, GGATCCC or GGGATCC) had to be removed from the experiments, as they ran the risk of creating staggered duplexes instead of the desired hairpin structure.
- 256 sequences with complementary bases in positions 3 and 5 were removed because they could form stable duplexes with a single mismatch pair.

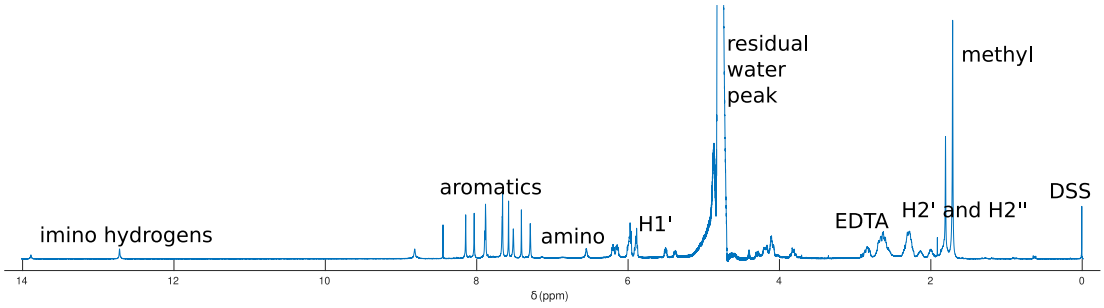

Figure 5.1: Representative 1D spectrum of an oligonucleotide, taken from the water suppression experiments with the CTTm^{5}CGAAG sequence. The amino hydrogens are distinguished by the change of chemical shift with temperature, rather than by the region of the shift itself.

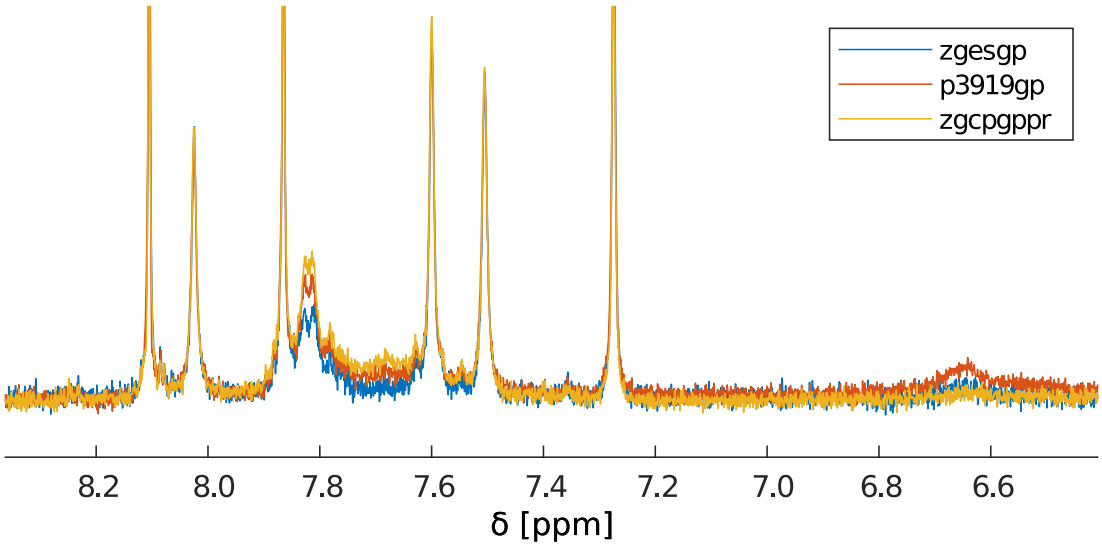

Figure 5.2: The aromatic range of the model ^{1}H NMR spectrum. While most peaks far away from water are comparable in all sequences, zgesgp performs worst in the C1H6 peak at 7.8 ppm. The exchangeable peak at 6.6 ppm is best visible in the p3919gp sequence.

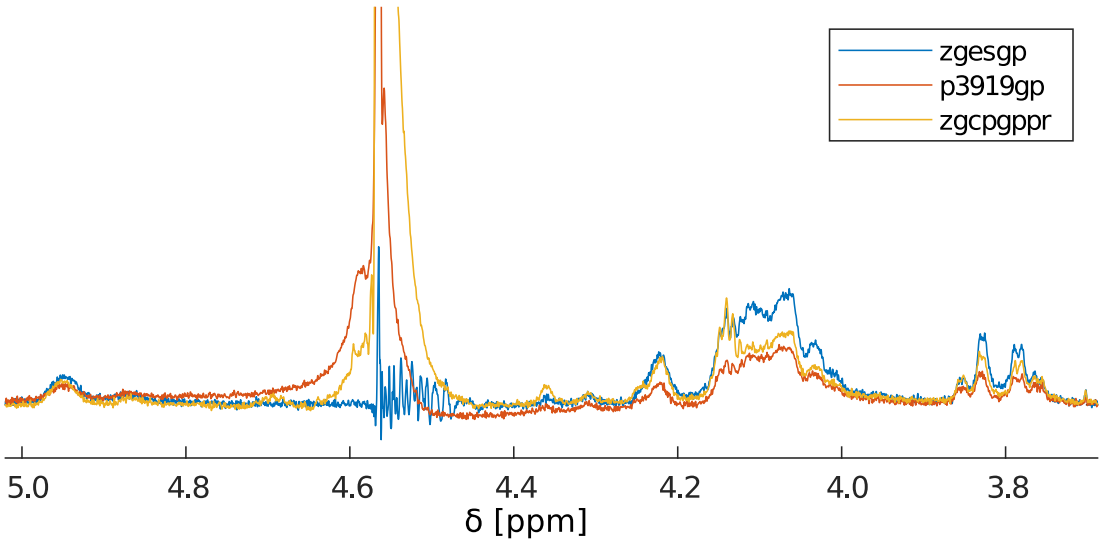

Figure 5.3: The water region of the NMR ^{1}H spectra of chosen water suppression sequences. zgesgp gives us highest sensitivity in the region to the left of the water peak, all pictured sequences are comparable on the right shoulder of the water peak. zgcpgppr has the biggest residual water peak.

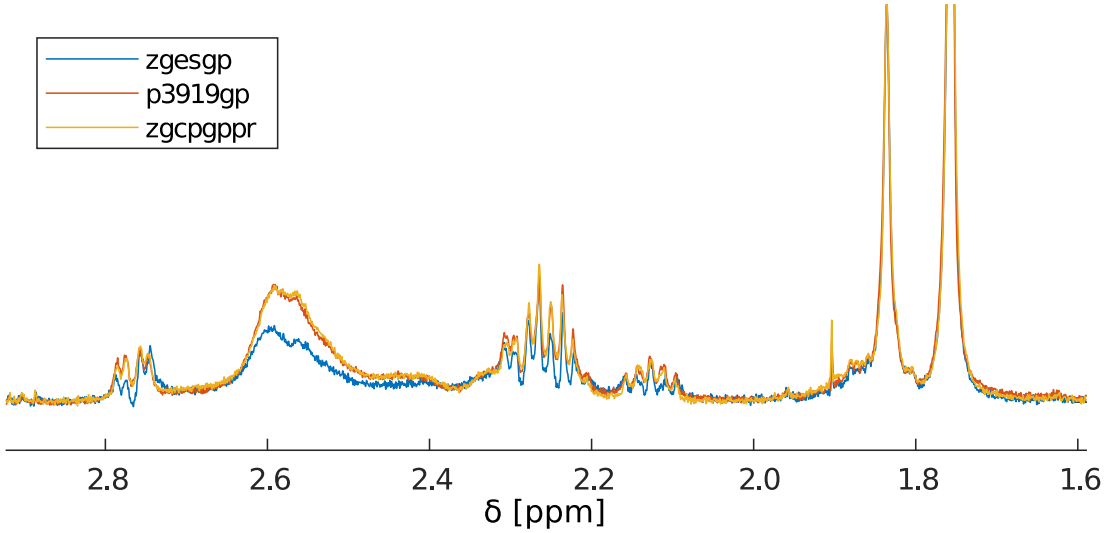

Figure 5.4: A significant loss of signal is present in the zgesgp NMR sequence here: the peak at 2.6 ppm is smaller than in any other sequence class pictured, and the echo has introduced an antiphase contribution which distorts the baseline in multiplets.

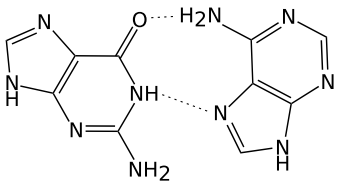

Figure 5.5: Pairing between the guanine Watson-Crick edge and adenine Hoogsteen edge

Even though it fits our criteria, one of the candidate sequences, GCGTAGC, has been shown[20] to form both hairpins and duplexes, showing that the method is not foolproof. These conditions narrow the search for suitable candidates down from 1024 to 744. The candidate structures were run through the DINAMelt package[26], which revealed that only 31 of them can form stable hairpins above the triple point of water. Judging from the melting temperatures calculated by the package, the rest is unstable because an A·T pair in the positions 2 and 6, with its two hydrogen bonds, doesn't provide enough structural integrity.

Our goal is not only to predict which 7-member oligonucleotides will form hairpins, but also the dependence of their thermodynamic properties on the sequence. One study[19] scanned through the space of 64 GCNNNGC oligonucleotides by plotting their resistance towards DNA polymerase against their mobility on polyacrylamide gel during electrophoresis, and found that only the ones with GNA central motif formed stable hairpins.

Structures with the A3-G5 (but not G5-A3) pair were selected against. Pairing between adenine and guanine would create only a single hydrogen bond, whereas the pairing between guanine and adenine creates two as per Fig. 5.5. Molecular dynamics[32] have shown that the bend in the GNA triplet is realized by stacking of the center nucleotide on guanine.

DINAMelt was unable to calculate the differences in the fourth position in the oligonucleotide, but it did show a mild preference for purine-pyrimidine stacking. Experiments on longer sequences[33], however, show preference for hairpins with the central motive GYA (GCA or CTA), and for duplexes with GRA (GGA, GAA). Overall, a GNA triplet is a necessary condition for short hairpins.

Table 5.1: A complete list of heptanucleotides capable of forming hairpins

AGGAACT	TGGAACA	CCGAAGG	GGGAACC
AGGGACT	TGGGACA	CCGGAGG	GGGGACC
AGGCACT	TGGCACA	CCGCAGG	GGGCACC
AGGTACT	TGGTACA	CCGTAGG	
ACGAAGT	TCGAAGA	CGGAACG	GCGAAGC
ACGGAGT	TCGGAGA	CGGGACG	GCGGAGC
ACGCAGT	TCGCAGA	CGGCACG	GCGCAGC
ACGTAGT	TCGTAGA	CGGTACG	GCGTAGC

This results in the 31 candidate structures in table 5.1. Note that the sequence GGGTACC is omitted, because it can form a staggered duplex.

In the end, we selected two sequences with the central GTA loop, with the closing base pairs C·G due to their high predicted stabily. The two sequences, CGGTACG and GCGTAGC, used in this work allow the study of the effect of the stem on the overall hairpin properties.

5.3 Resonance assignment

We measured NOESY spectra for both samples at 288 K. This was sufficient for peak assignment in the aromatic region of the George sample. Fig. 5.6 depicts the assignment in the H1' region, and Fig. 5.7 depicts the assignment in the H2'/H2" that was done to fill in the gaps and help with the assignment of guanine aromatics.

However, the 288 K NOESY alone wasn't sufficient for clear assignment in the Charlie oligonucleotide. Fig. 5.8 shows the presence of too many crosspeaks, hinting at a second structure and obscuring the NOESY spectrum of the desired hairpin. Two more NOESY experiments were needed for unambiguous assignment: a spectrum at 298 K (depicted on Figs. 5.9 and 5.10) provided most crosspeaks, but left some uncertainty in cytosines, which weren't resolved enough at that temperature. A 316 K spectrum didn't have many peaks remaining, but it ultimately helped resolve the difference between cytosine aromatic nuclei C1H6 and C6H6 (Fig. 5.11).

It can be shown in the NOESY spectra that the secondary structures are more likely hairpins than B-DNA duplexes. The crosspeaks between A5H8 and T4H1', T4H2', and T4H2" for both Georgeand Charlieare weaker than other crosspeaks between an aromatic hydrogen and the deoxyribose from the previous residue. In B-DNA, the same part of the molecule would be much more rigid, and the same peaks more clearly resolved.

Now we have a complete aromatic assignment for both oligonucleotides that we will use further in the melting analysis.

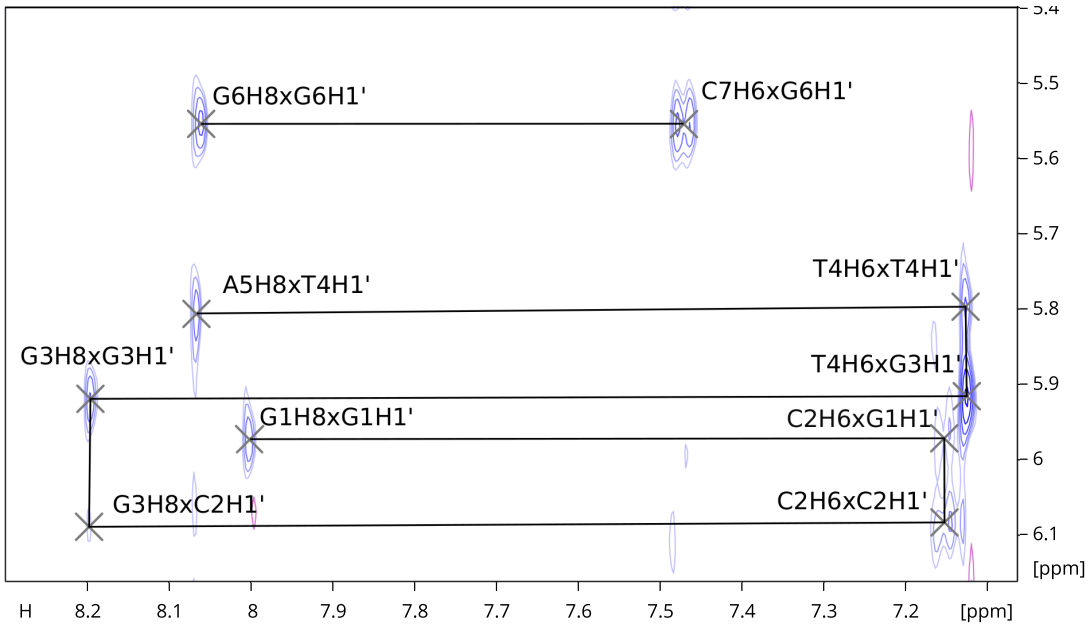

Figure 5.6: George (GCGTAGC) NOESY at 288 K. Note the missing A5H1' crosspeaks with A5H8 and G6H8: their chemical shifts are too close to each other at this temperature for any decisive crosspeaks.

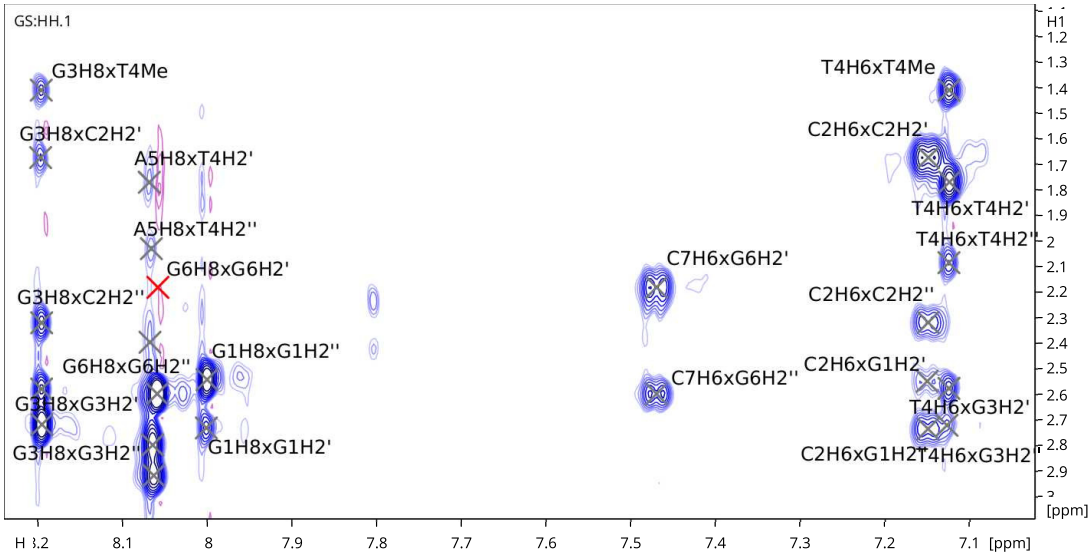

Figure 5.7: George NOESY at 288 K in the H2' and H2" region. Lines connecting crosspeaks with the same shift in one dimension have been omitted for clarity. The missing crosspeaks between the A5 and the G6 residue are a consequence of the close chemical shifts of the aromatic nuclei.

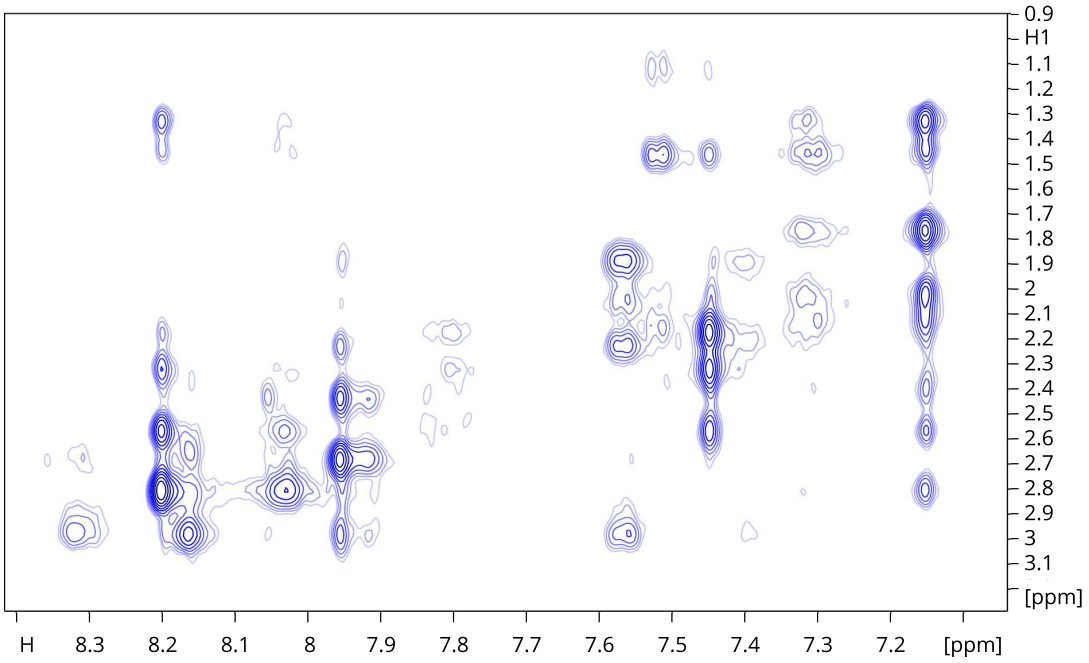

Figure 5.8: Charlie (CGGTACG) NOESY at 278 K in the H2' and H2" region. 16 groups of signals along the aromatic x axis show that there is slow exchange between hairpin, and another secondary structure with broad peaks.

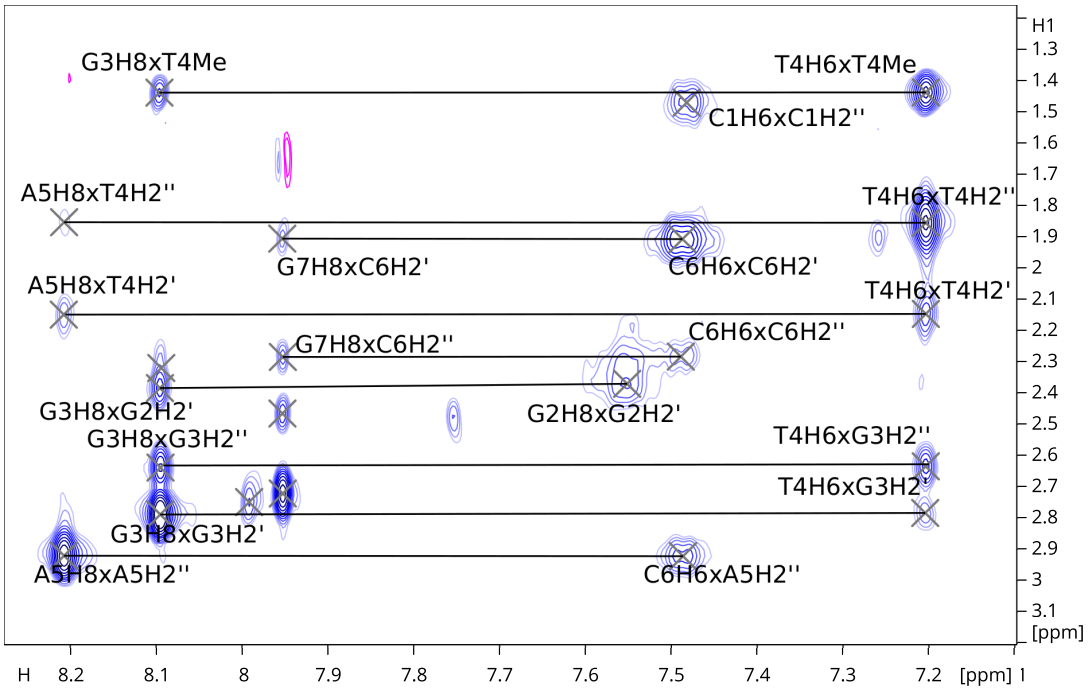

Figure 5.9: Charlie NOESY at 298 K in the H2' and H2" region with assignments. The C1H6 and the C6H6 peaks overlap.

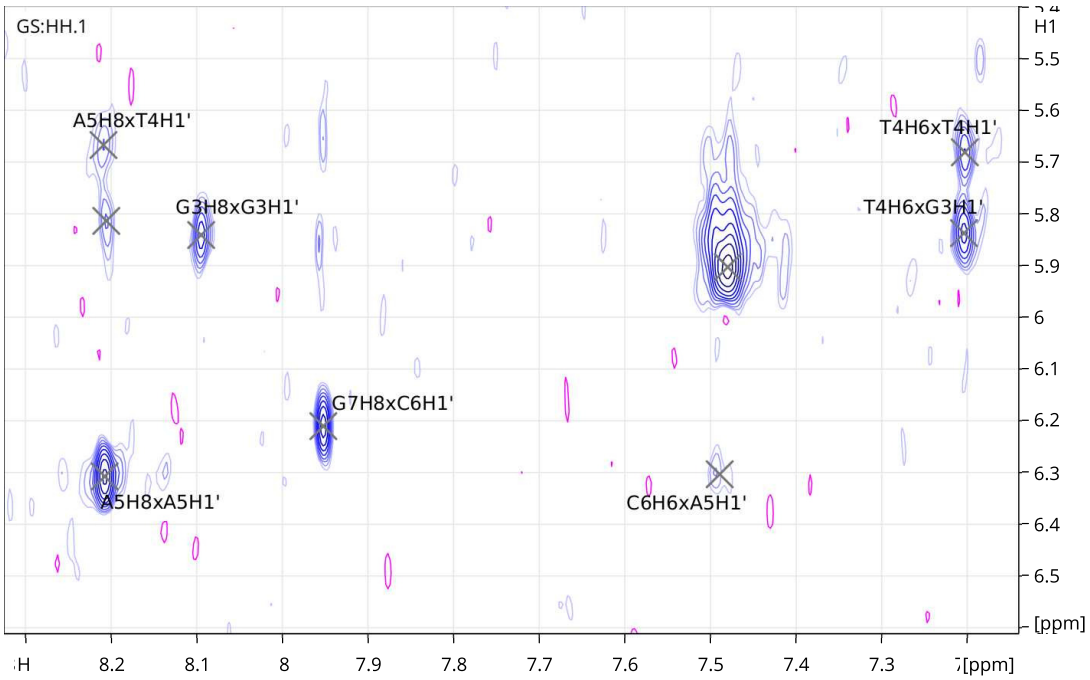

Figure 5.10: Charlie (CGGTACG) NOESY at 298 K in the H1' region. The missing broad peaks of G2H8, and the overlap of C1H6 and C6H6 aromatic shifts limit the possibility of assignments from this region of the NOESY spectrum.

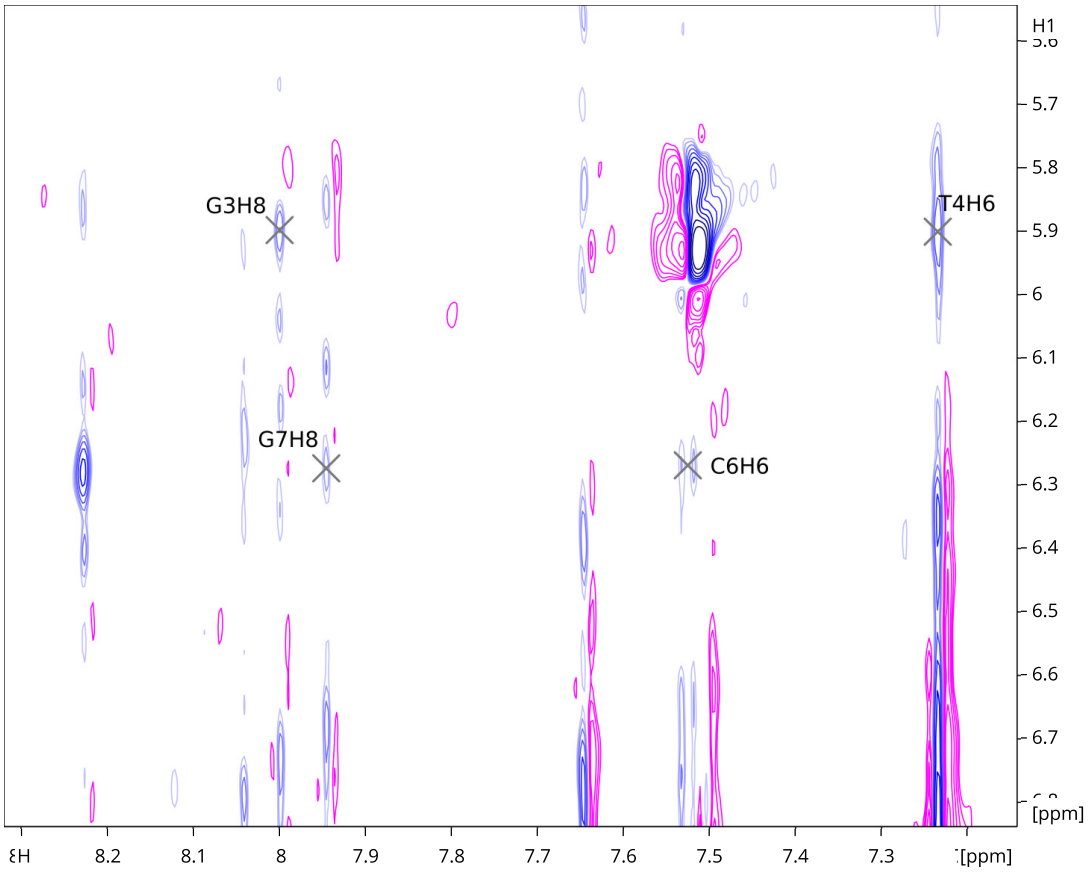

Figure 5.11: Charlie NOESY at 316 K in the H1' region, used to differentiate between the C6H6 and the C1H6 chemical shifts.

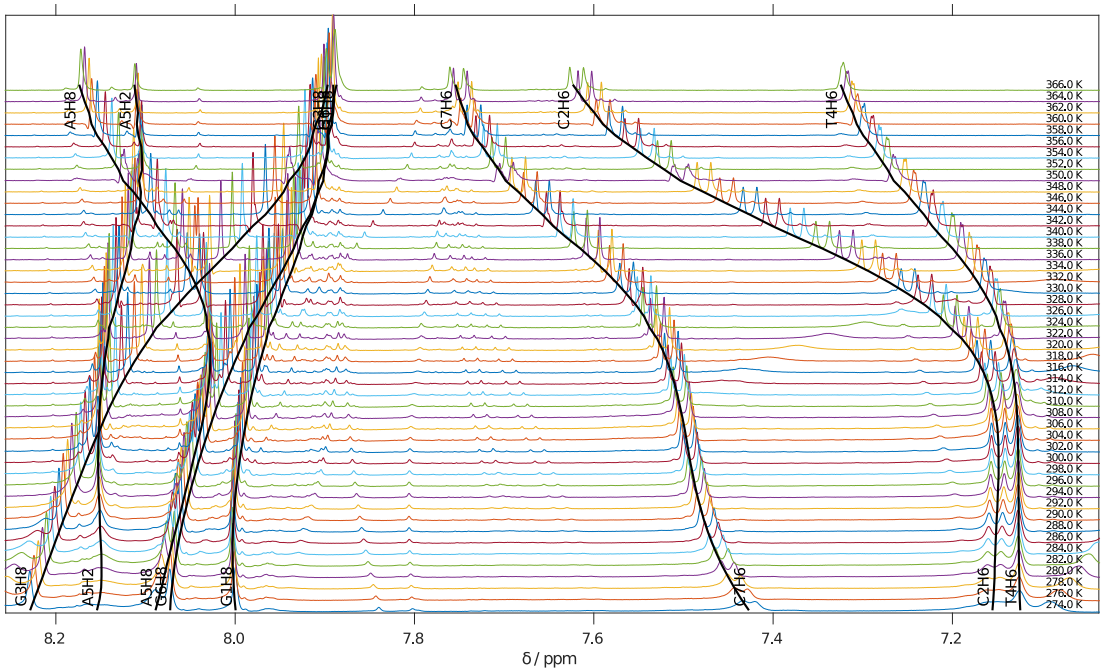

Figure 5.12: Temperature series for the George sample in the aromatic region of the NMR spectra

5.4 Temperature dependent spectra

The George sample was measured at a single concentration of 1.15 mM. Its temperature series is pictured in Fig. 5.12. Each of the 47 spectra was fitted to a linear combination of Lorentz curves. The Charlie sample was initially measured at a concentration of 1.66 mM (Fig. 5.13). This variable temperature series achieved slow chemical exchange between a hairpin and an unknown secondary structure up until 292 K. To differentiate the effect of the hairpins from the effect of possible complexes of multiple molecules, a second series of NMR experiments at a concentration of 0.28 mM was also included (Fig. 5.14). The tracing of the fast exchange peaks was therefore done separately for each of the two sets of peaks. The hairpin and the other set of peaks (that was assumed to be a duplex) could be distinguished both by the continuity of the tracing of the peaks across the spectra, and the lower amplitude and broader peaks of the complex. The result was fitted to a sum of Lorentz peaks with the help of the Asymexfit[34] package.

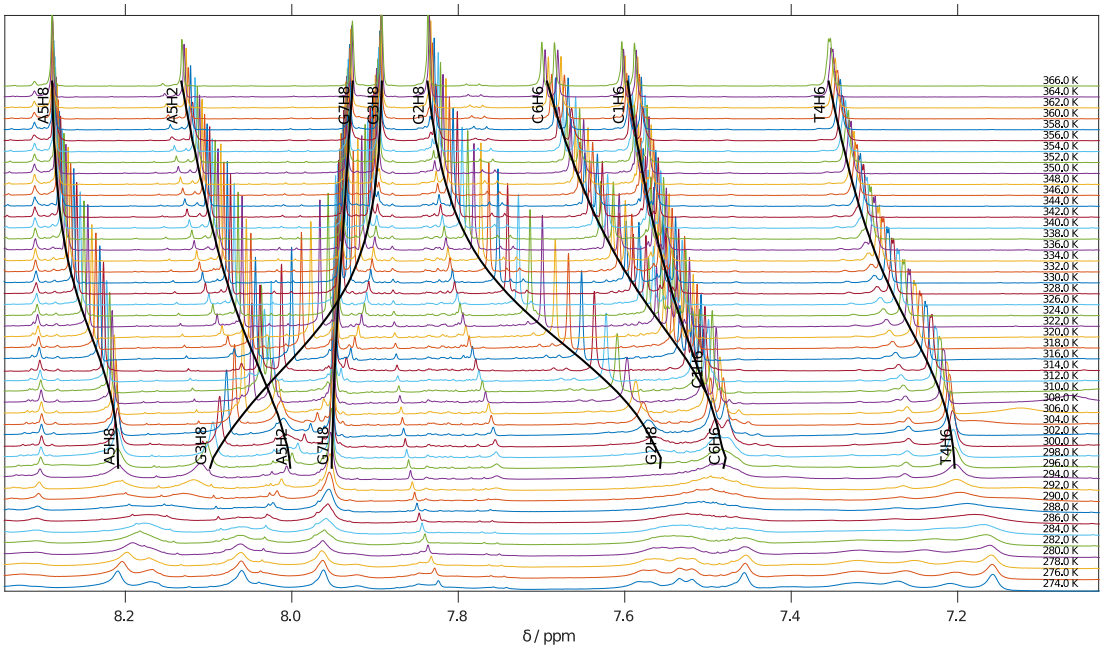

Figure 5.13: Temperature series for the Charlie sample in the aromatic region of the NMR spectra

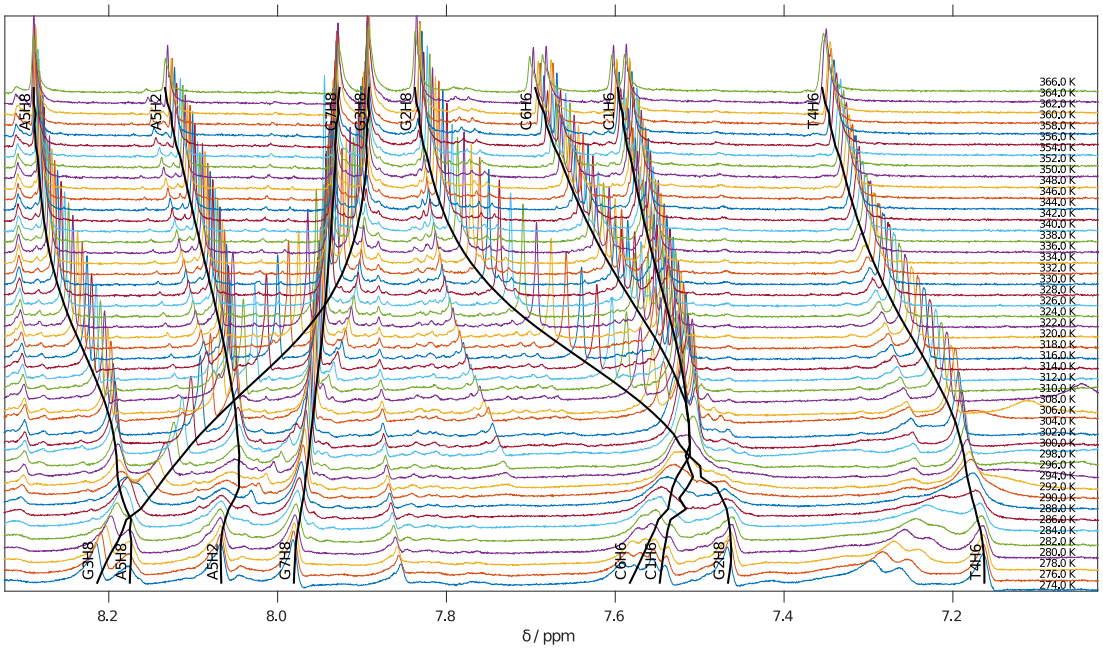

Figure 5.14: Temperature series for the Charlie 0.2 sample in the aromatic region of the NMR spectra

Table 5.2: Thermodynamic parameters for each nucleus

	ΔH / kJ · mol^{-1}	ΔS / J · mol^{-1} · K^{-1}	ΔG_{310K} / kJ · mol^{-1}	T_m / K
Charlie - CGGTACG at 1.66 mM				
C1H6	-57 ± 32	-193 ± 55	3 ± 36	294 ± 162
G2H8	-90 ± 4	-283 ± 10	-2 ± 5	317 ± 2
G3H8	-87 ± 3	-275 ± 10	-2 ± 5	316 ± 2
T4H6	-90 ± 9	-285 ± 29	-2 ± 13	316 ± 2
A5H2	-88 ± 14	-286 ± 37	1 ± 18	307 ± 13
A5H8	-92 ± 9	-291 ± 26	-2 ± 12	318 ± 2
C6H6	-83 ± 7	-262 ± 22	-2 ± 10	316 ± 2
G7H8	-102 ± 142	-326 ± 472	-1 ± 204	312 ± 27
Charlie 02 - CGGTACG at 0.25 mM				
C1H6	-84 ± 47	-261 ± 143	-3 ± 65	321 ± 7
G2H8	-89 ± 4	-281 ± 12	-2 ± 6	316 ± 2
G3H8	-81 ± 4	-256 ± 12	-2 ± 5	319 ± 1
T4H6	-84 ± 23	-269 ± 68	-1 ± 31	313 ± 7
A5H2	-31 ± 126	-107 ± 353	2 ± 167	289 ± 234
A5H8	-91 ± 12	-289 ± 34	-2 ± 16	315 ± 3
C6H6	-76 ± 16	-241 ± 49	-1 ± 22	315 ± 5
G7H8	-38 ± 76	-110 ± 182	-4 ± 95	343 ± 484
George - GCGTAGC at 1.15 mM				
G1H8	-52 ± 4	-150 ± 13	-6 ± 6	358 ± 15
C2H6	-100 ± 1	-292 ± 5	-9 ± 2	341 ± 0
G3H8	-103 ± 3	-303 ± 8	-9 ± 4	341 ± 1
T4H6	-100 ± 3	-294 ± 10	-9 ± 5	341 ± 1
A5H2	-94 ± 7	-276 ± 22	-8 ± 10	340 ± 1
A5H8	-97 ± 3	-284 ± 8	-9 ± 4	341 ± 1
G6H8	-67 ± 3	-195 ± 11	-7 ± 5	346 ± 3
C7H6	-115 ± 3	-338 ± 10	-10 ± 5	341 ± 1

5.5 Thermodynamic properties

The chemical shifts of aromatic protons with respect to temperature, obtained in the previous part, were then fitted by the melting curve according to Eq. 3.17. Linewidths served as error estimates of the shifts and were used in the fit as weights. The results are shown in Figs. 5.15, 5.16, and 5.17. Thanks to that we obtained a set of thermodynamic parameters ΔH, ΔS, ΔG, T_m in Table 5.2 and their errors, for each nucleus. Judged separately, they seem arbitrary. Together, they show us a picture of the melting process. Graphs 5.19 and 5.18 reveal that the melting temperatures do not vary significantly along the length of our hairpins.

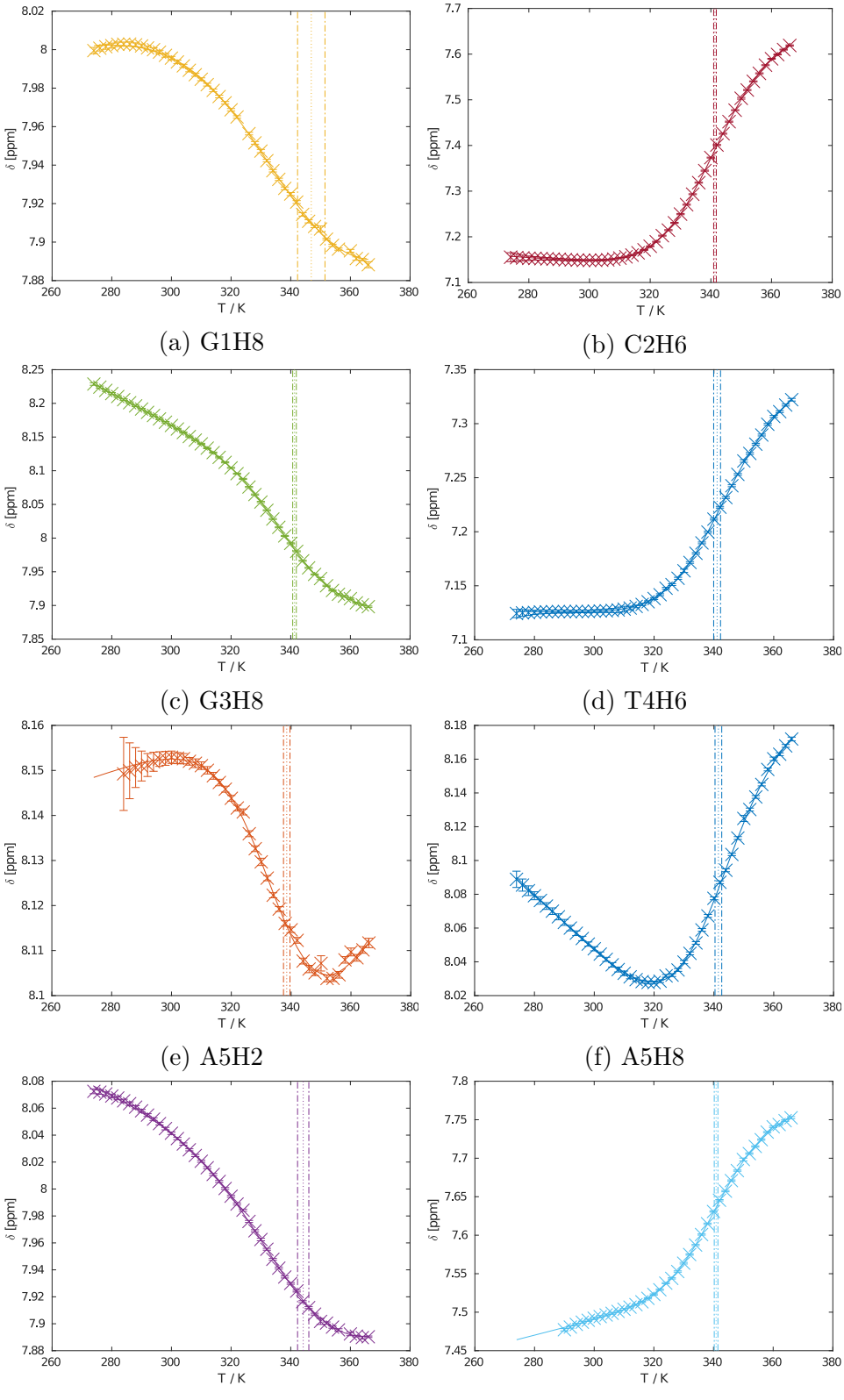

(a) G1H8 (b) C2H6

(c) G3H8 (d) T4H6

(e) A5H2 (f) A5H8

(g) G6H8 (h) C7H6

Figure 5.15: Plots of chemical shift against temperature for the aromatic ^{1}H nuclei in the George sample, together with a fit curve for each.

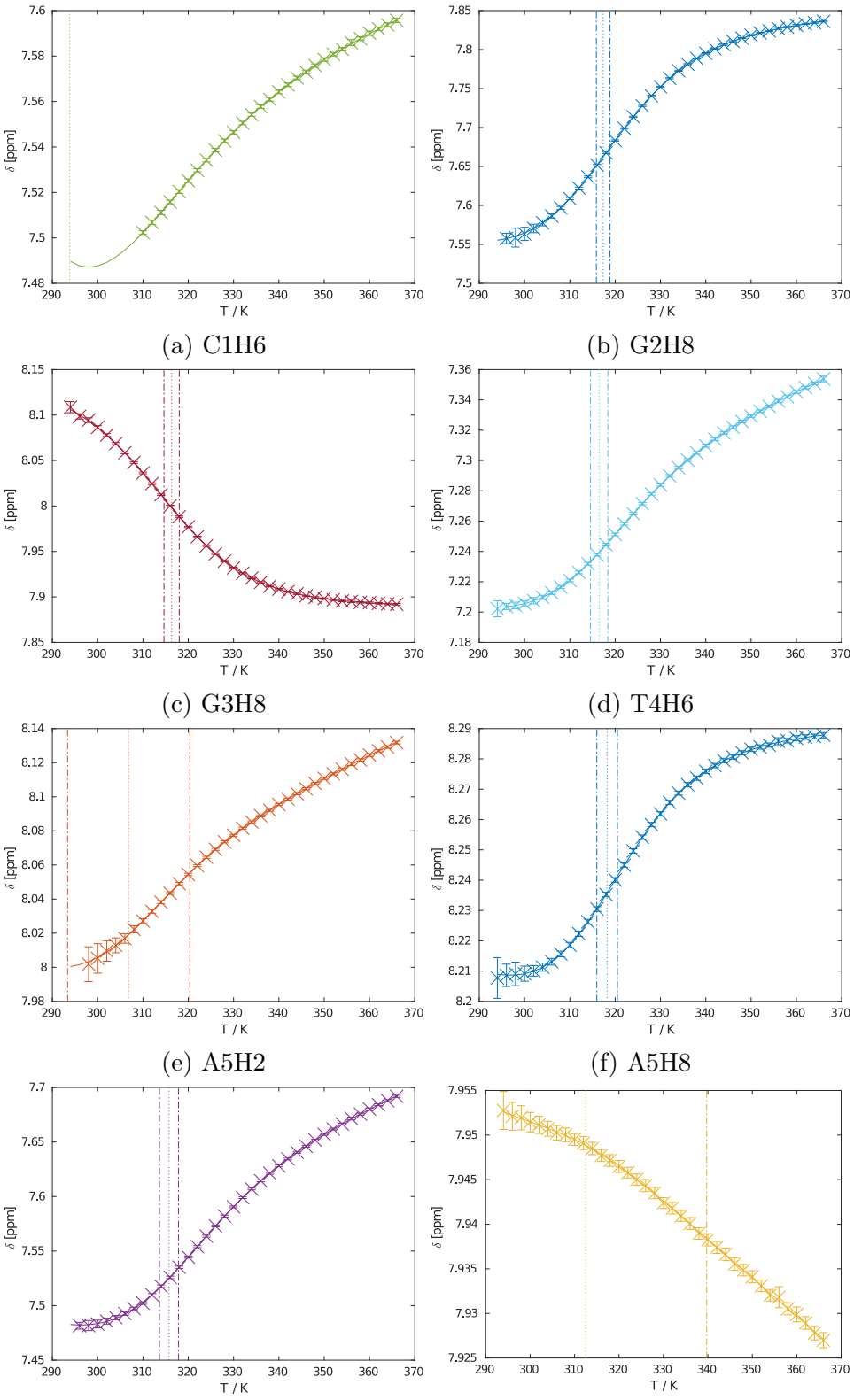

(a) C1H6 (b) G2H8

(c) G3H8 (d) T4H6

(e) A5H2 (f) A5H8

(g) C6H6 (h) G7H8

Figure 5.16: Plots of chemical shift against temperature for the aromatic ^{1}H nuclei in the Charlie sample, together with a fit curve for each.

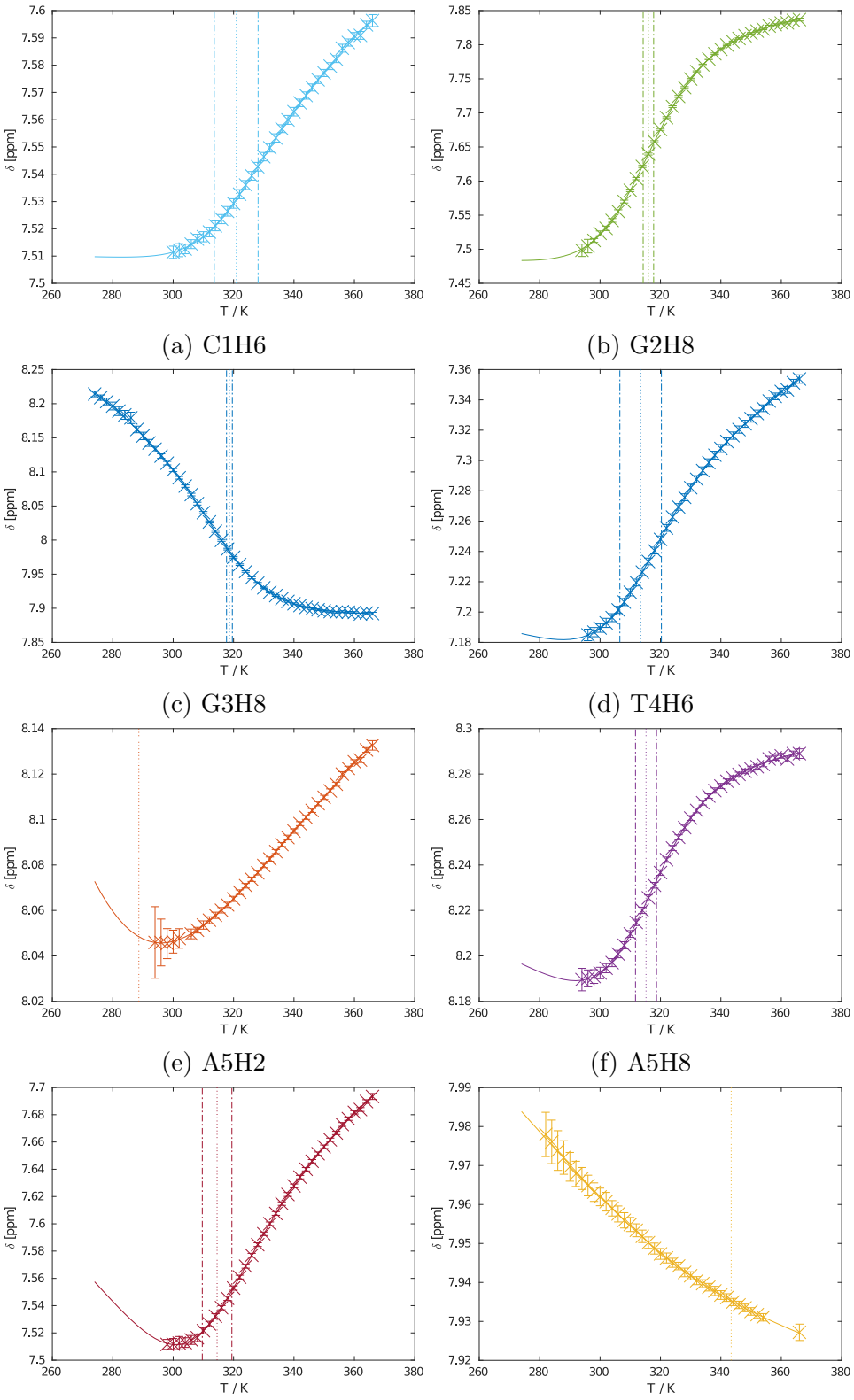

(a) C1H6 (b) G2H8

(c) G3H8 (d) T4H6

(e) A5H2 (f) A5H8

(g) C6H6 (h) G7H8

Figure 5.17: Plots of chemical shift against temperature for the aromatic ^{1}H nuclei in the Charlie 0.2 sample, together with a fit curve for each.

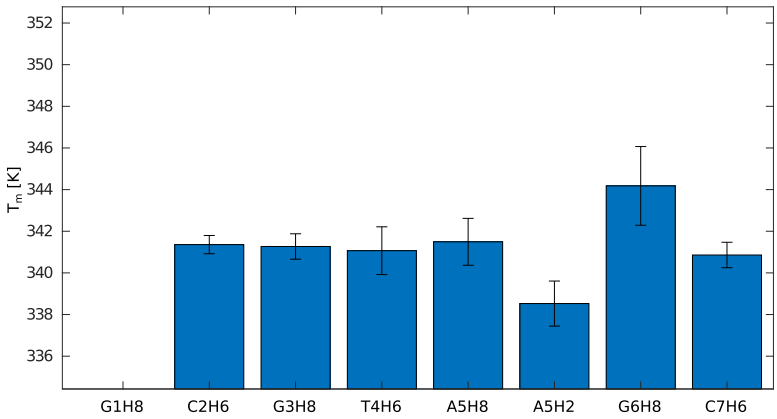

Figure 5.18: Melting temperatures obtained for each aromatic ^{1}H nucleus in the George sample. The nuclei where the fit wasn't possible are not included.

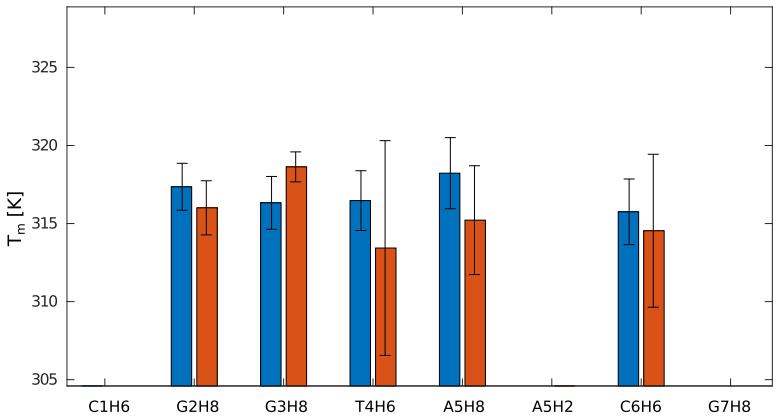

Figure 5.19: Melting temperatures obtained for each aromatic ^{1}H nucleus in the Charlie sample for both concentrations. The nuclei where the fit wasn't possible are not included.

6. Discussion

6.1 The formation of secondary structures

The Charlie oligonucleotide was measured at two different concentrations. At each of these concentrations, the melting temperature T_m was determined for each nucleus from variable temperature NMR. The consensus melting temperature is 44 °C in both concentrations, with a uniform melting profile along the strand. Because the melting temperature doesn't depend on concentration, the secondary structure is unimolecular. A comparison between the melting curves of two example nuclei in both concentration is provided in Fig. 6.1. Comparison of χ^2 for a hairpin model and a duplex model favors the hairpin. A plot of fit residues is shown in Fig. 6.4.

The Charlie strand has been observed by us to also form a secondary structure, as shown by the presence of 16 distinct peaks up until 288 K. One such spectrum is pictured in Fig. 6.2. This secondary structure might be a duplex, with a drastically lower T_m, as it entirely disappears at lower concentrations. As was the case in the previous oligonucleotide, chi^2 favors the hairpin over duplex.

We measured the George sample at a single concentration, which alone was sufficient in determining the formation of hairpin with a uniform melting temperature of 68°C along the whole strand. A second most likely option was the formation of duplexes, which was disproven by obtaining thermodynamic parameters with an assumption of a duplex (Fig. 6.3). Comparison of χ^2 for the duplex model and for the hairpin model favors the hairpin.

Literature reports a duplex formation within the George strand[20] in 5.7 mM solution. No reference to hairpin and duplex formation was found for the Charlie oligonucleotide sequence. We haven't observed George duplex due to the abnormal stability of its hairpin, and the apparent higher concentrations required for duplex formation.

Therefore, Charlie and George both form stable hairpins.

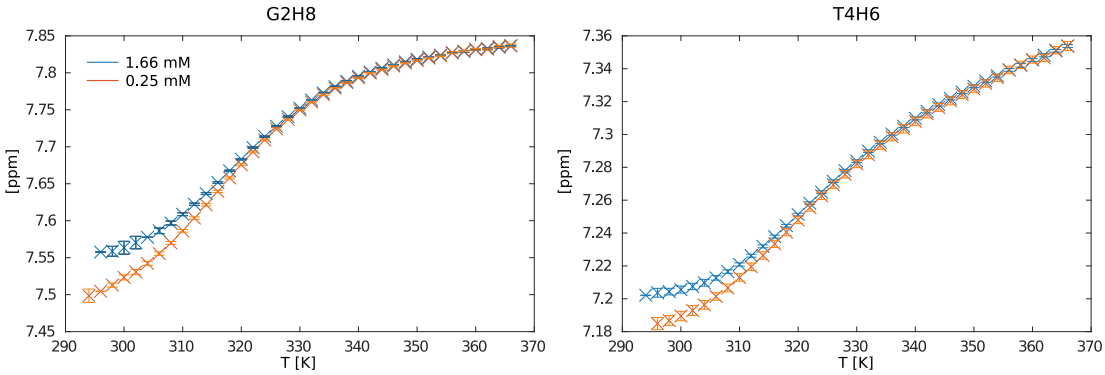

Figure 6.1: Comparison of the melting curves of two different nuclei in both concentrations measured for the Charlie sample. The melting temperature T_m remains unchanged, because the structure observed is a hairpin.

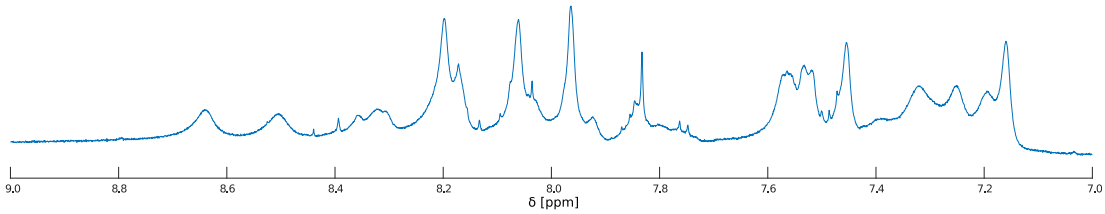

Figure 6.2: The aromatic segment of a Charlie NMR spectrum at 278 K. The broad signals of the duplex are easily discernible from the peaks of the hairpin.

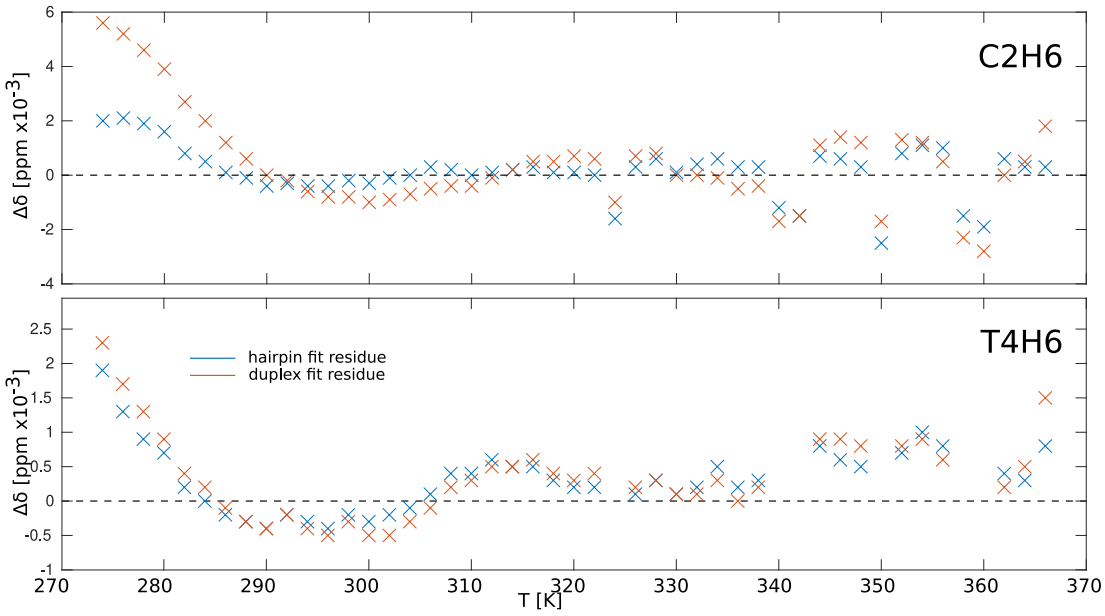

Figure 6.3: Comparison of melting curve fit residues in a model that assumes the formation of a hairpin (blue) and the formation of a duplex (orange) in the George sequence.

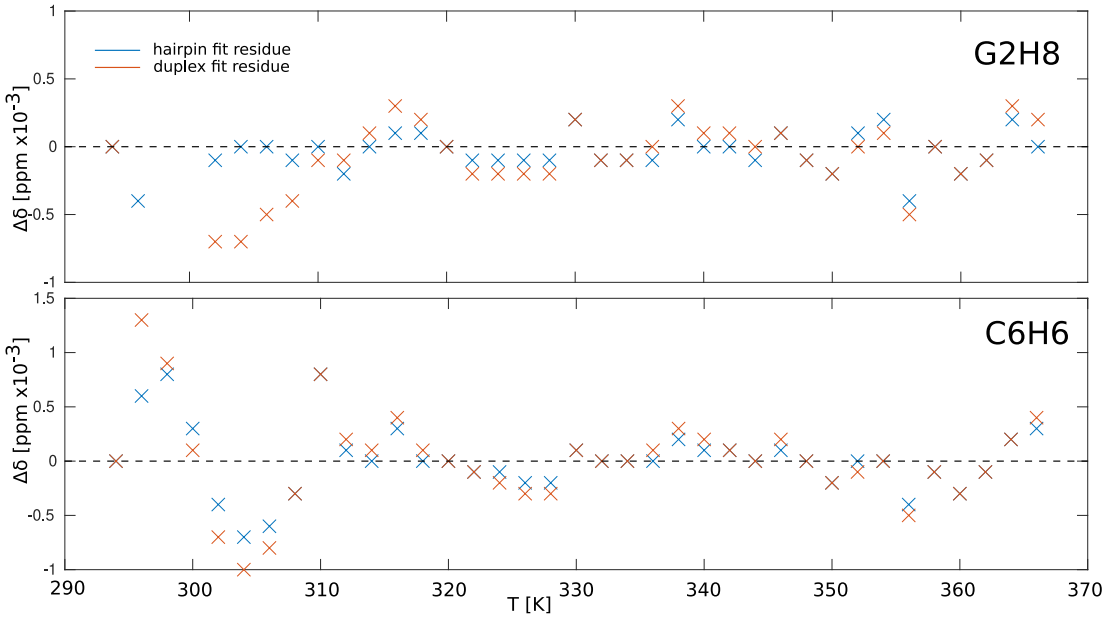

Figure 6.4: Comparison of melting curve fit residues in a model that assumes the formation of a hairpin (blue) and the formation of a duplex (orange) in the Charlie sequence.

6.2 Comparison of stability with the nearest-neighbor model

Both our measurements and the nearest-neighbor model agree that the melting temperature of Charlie is lower than the melting temperature of George. The model's parameters[25] and the experimental evidence[35] point towards the stacking of alternating purines and pyrimidines (such as the GCG motif of George) resulting in more stable structures than stacking without alternating (as is the case in the Charlie sequence with its CGG stem motif). The nearest-neighbor energy difference for the 5A-6G in George and 5A-6C in Charlie is smaller than the difference between 2C-3G (Charlie) and 2G-3G (George), which is why the second term is a more decisive factor in the stability of the hairpin, and the Charlie strand melts at lower temperatures than the Georgestrand.

The nearest-neighbor model[26] predicts a 54°C melting temperature for Charlie (instead of the 44 °C measured) and 58°C for George (instead of 68°C). The experiments have successfully shown that the existing models provide qualitative prediction for the creation of hairpins. The accuracy of these melting temperatures, however, is only 10 Kelvin. As the model predicts the same melting temperatures for oligonucleotides which differ by the central nucleotide in the loop, the discrepancy can be expected to be even larger for more stable hairpin loops than the GTA triplet in Charlie and George.

The difference between the model and the experiment can be explained by the limitations of the nearest neighbor model outlined in 1998[25], which only accounts for hydrogen bonded pairs, and assigns a flat penalty for unbound bases. Terms for stacking of the unbound nucleotides with bound ones are not included in the nearest-neighbor model.

6.3 Comparison with T_m from previous experimental results

While they were not involved in the experimental part of this thesis, other, similar oligonucleotides are part of the broader scope of understanding of the formation of hairpins. Table 6.1 depicts results of two teams with the GCGNAGC[36][19] family of oligonucleotides. It shows an 8°C difference between the least stable chain and the most stable one. While they are consistent with each other, there is a small difference between their T_m and ours, likely arising from a different buffer formula. However, it hints at a trend that could be present in all NNGNANN hairpin candidates. As no melting temperature data for other minihairpins than the ones mentioned in Table 6.1 is available, this area remains mostly unexplored.

Table 6.1: Comparison of relevant oligonucleotides T_m.

	Rosemeyer, 2004[36]	Yoshizawa, 1997[19]	this thesis
GCGAAGC	72	72.3	
GCGGAGC	71	70.5	
GCGCAGC	67	67	
GCGTAGC	66	66.3	68
CGGTACG			43

Conclusion

The aim of this thesis was to evaluate the formation of stable mini-hairpins by NMR variable temperature experiments. This was done by assessing the candidate mini-hairpin sequences by a nearest-neighbor theoretical model, and comparing the prediction with experimentally obtained thermodynamic parameters.

- 31 DNA strands forming stable minihairpins were selected with the aid of the nearest-neighbor model out of a pool of 1024 possible candidates.
- Two sequences, CGGTACG (referred to as Charlie in the thesis) and GCGTAGC (referred to as George) which differ only by the order of the first two base pairs were chosen for measurement.
- We measured NOESY spectra of these two speciments for signal assignment.
- Once assigned, the peaks in the aromatic region were measured across a range of temperatures from 274 K to 266 K.
- Melting curves were obtained from the 1D spectra by extracting data about chemical shifts and spectral line widths from the temperature series.
- The thermodynamic parameters of the aromatic nuclei were obtained, giving us information about the stability and melting temperatures.

We have been able to show that the two selected candidate structures, George and Charlie, do indeed form stable hairpins. As per the theoretical prediction, their melting temperatures T_m are vastly different from each other due to the stabilizing effect of stacking alternating purine and pyrimidine bases in George (in the form of the GCGNNGC motif), resulting in a 25 K melting temperature difference between the two. The melting temperature is uniform along the whole strand for both hairpins. The obtained T_m differ from the model in opposite directions, suggesting that some other interactions, not included in the nearest neighbor model, are at play.

Bibliography

[1] A Roulston, P Beauparlant, N Rice, and J Hiscott. Chronic human immunodeficiency virus type 1 infection stimulates distinct NF-kappa B/rel DNA binding activities in myelomonoblastic cells. *Journal of Virology*, 67(9), 1993.

[2] Hasan Uludağ, Kylie Parent, Hamidreza Montazeri Aliabadi, and Azita Haddadi. Prospects for RNAi Therapy of COVID-19, 2020.

[3] David Bikard, Céline Loot, Zeynep Baharoglu, and Didier Mazel. Folded DNA in Action: Hairpin Formation and Biological Functions in Prokaryotes. *Microbiology and Molecular Biology Reviews*, 74(4):570–588, 2010.

[4] Libuše Trnková, Irena Postbieglová, and Miroslav Holik. Electroanalytical determination of d(GCGAAGC) hairpin. *Bioelectrochemistry*, 63(1-2):25–30, jun 2004.

[5] Jean Chatain, Alain Blond, Anh Tuân Phan, Carole Saintomé, and Patrizia Alberti. GGGCTA repeats can fold into hairpins poorly unfolded by replication protein A: a possible origin of the length-dependent instability of GGGCTA variant repeats in human telomeres. *Nucleic Acids Research*, jul 2021.

[6] Nicolas Foloppe, Brigitte Hartmann, Lennart Nilsson, and Alexander D. MacKerell. Intrinsic conformational energetics associated with the glycosyl torsion in DNA: A quantum mechanical study. *Biophysical Journal*, 82(3):1554–1569, mar 2002.

[7] Neocles B. Leontis and Eric Westhof. Geometric nomenclature and classification of rna base pairs. *RNA*, 7(4):499–512, 2001.

[8] Neocles B. Leontis, Jesse Stombaugh, and Eric Westhof. The non-Watson–Crick base pairs and their associated isostericity matrices. *Nucleic Acids Research*, 30(16):3497–3531, 08 2002.

[9] V. Kumar, V. Kesavan, and K. V. Gothelf. Highly stable triple helix formation by homopyrimidine (l)-acyclic threoninol nucleic acids with single stranded DNA and RNA". *Organic & Biomolecular Chemistry*, 13(8):2366–2374, 2015.

[10] Wesley I. Sundquist and Aaron Klug. Telomeric DNA dimerizes by formation of guanine tetrads between hairpin loops. *Nature*, 342(6251), 1989.

[11] D. M.J. Lilley. Structures of helical junctions in nucleic acids, may 2000.

[12] R. E. Franklin and R. G. Gosling. The structure of sodium thymonucleate fibres. I. The influence of water content. *Acta Crystallographica*, 6(8–9):673–677, 1953.

[13] O. Socha. *Charakterizase strukturních vlastností a stability DNA vlásenek pomocí NMR spektroskopie*. Diploma thesis, Charles University, 2016.

[14] R. Sgallová. *Termodynamika tvorby DNA vlásenek*. Diploma thesis, Charles University, 2019.

[15] A Marquis Gacy, Geoffrey Goellner, Nenad Juranic, Slobodan Macura, and Cynthia T Mcmurray. Trinucleotide Repeats That Expand in Human Disease Form Hairpin Structures In Vitro. Technical report, 1995.

[16] Brooke L. Heidenfelder, Alexander M. Makhov, and Michael D. Topal. Hairpin Formation in Friedreich's Ataxia Triplet Repeat Expansion. *Journal of Biological Chemistry*, 278(4), jan 2003.

[17] Linxi Zhang and Tingting Sun. Statistical properties of nucleotides in human chromosomes 21 and 22. *Chaos, Solitons & Fractals*, 23(3), feb 2005.

[18] Srinivasaraghavan Kannan and Martin Zacharias. Role of the closing base pair for d(GCA) hairpin stability: free energy analysis and folding simulations. *Nucleic Acids Research*, 39(19), oct 2011.

[19] Satoko Yoshizawa, Gota Kawai, Kimitsuna Watanabe, Kin Ichiro Miura, and Ichiro Hirao. GNA trinucleotide loop sequences producing extraordinarily stable DNA minihairpins. *Biochemistry*, 36(16):4761–4767, apr 1997.

[20] Eveline Lescrinier, Shuqun Sheng, Jan Schraml, Roger Busson, and Piet Herdewijn. d(GCGTAGC), an equilibrium between a hairpin structure and an unusual duplex. *Nucleosides and Nucleotides*, 18(11-12):2721–2744, 1999.

[21] T. Sunami, J. Kondo, M. Tsunoda, T. Sekiguchi, I. Hirao, K. Watanabe, K.-i. Miura, and A. Takenaka. X-ray structure of d(GCGAAGC); Switching of partner for G:A pair in duplex form. *Nucleic Acids Symposium Series*, 2(1), nov 2002.

[22] Reinhard Bauer, Axel Imhof, Armin Pscherer, Heidrun Kopp, Markus Moser, Silvia Seegers, Monika Kerscher, Michael A. Tainsky, Ferdinand Hofstaedter, and Reinhard Buettner. The genomic structure of the human AP-2 transcription factor. *Nucleic Acids Research*, 22(8), 1994.

[23] Ruth Nussinov. Some guidelines for identification of recognition sequences: Regulatory sequences frequently contain (T)GTG/CAC(A), TGA/TCA and (T)CTC/GAG(A). *BBA - Gene Structure and Expression*, 866(2-3):93–108, mar 1986.

[24] V. Římal. *NMR study of oligonucleotide structures*. Phd thesis, Charles University, 2018.

[25] J. SantaLucia. A unified view of polymer, dumbbell, and oligonucleotide DNA nearest-neighbor thermodynamics. *Proceedings of the National Academy of Sciences*, 95(4), feb 1998.

[26] Nicholas R Markham and Michael Zuker. DINAMelt web server for nucleic acid melting prediction. *Nucleic Acids Research*, 33(Web Server issue):W577–W581, 2005.

[27] Malcolm H Levitt. *Spin dynamics: basics of nuclear magnetic resonance*. Wiley, New York, NY, 2001.

[28] T. Hwang and A. Shaka. Water suppression that works. Excitation sculpting using arbitrary wave-forms and pulsed-field gradients. *Journal of Magnetic Resonance, Series A*, 2(112), 2 1995.

[29] Martial Piotto, Vladimir Saudek, and Vladimir Sklenář. Gradient-tailored excitation for single-quantum NMR spectroscopy of aqueous solutions. *Journal of Biomolecular NMR*, 2(6), 1992.

[30] Teodor Parella. *Pulse program catalogue: I. 1D & 2D NMR experiments*. Bruker BioSpin GmbH, Barcelona, 2008.

[31] Kurt Wüthrich. *NMR of proteins and nucleic acids*. John Wiley, Chichester, 1986.

[32] Petr Padrta, Richard Štefl, Lukáš Králík, Lukáš Žídek, and Vladimír Sklenář. Refinement of d(GCGAAGC) hairpin structure using one- and two-bond residual dipolar couplings. *Journal of Biomolecular NMR*, 24(1):1–14, sep 2002.

[33] Shan Ho Chou, Leiming Zhu, and Brian R. Reid. On the relative ability of centromeric GNA triplets to form hairpins versus self-paired duplexes. *Journal of Molecular Biology*, 259(3):445–457, jun 1996.

[34] V. Římal, H. Štěpánková, and J. Štěpánek. Analysis of NMR spectra in case of temperature-dependent chemical exchange between two unequally populated sites. *Concepts in magnetic resonance*, 38A(3):117–127, 2011.

[35] D. Ossipov, E. Zamaratski, and J. Chattopadhyaya. The 5'-Purine-Pyrimidine-3' Stacks are More Stabilizing in a Self-3'-Pyrinudine-Purine-5' complementary DNA Duplex than the 5'-Purine-Purine-3' 3'-Pyrimidine-Pyrimidine-5' Stack. *Nucleosides and Nucleotides*, 17(9-11), sep 1998.

[36] Helmut Rosemeyer, Verena Mokrosch, Anup Jawalekar, Eva Maria Becker, and Frank Seela. Single-Stranded DNA: Replacement of Canonical by Base-Modified Nucleosides in the Minihairpin 5′-d(GCGAAGC)-3′ and Constructs with the Aptamer 5′-d(GGTTGGTGTGGTTGG)-3′). *Helvetica Chimica Acta*, 87(2):536–553, feb 2004.

List of Figures

List of Tables

List of Abbreviations

A	adenine
C	cytosine
DNA	deoxyribonucleic acid
DSS	4,4-dimethyl-4-silapentane-1-sulfonic acid
FID	free induction decay
G	guanine
NMR	nuclear magnetic resonance
NOE	Nuclear Overhauser Effect
NOESY	Nuclear Overhauser Effect SpectroscopY
NS	number of scans
RNA	ribonucleic acid
T	thymine
TD	time domain
TMS	tetramethylsilane
WATERGATE	(WATER suppression by GrAdient Tailored Excitation)